archive

THE COMPARISON OF AVAILABLE DATA ON PWR ASSEMBLY THERMAL BEHAVIOR WITH ANALYTICAL PREDICTIONS

by

J. Liu, N. Todreas

Energy Laboratory Report No. MIT-EL 77-009
Draft: June 1977
Final: February 1979

THE COMPARISON OF AVAILABLE DATA ON PWR ASSEMBLY THERMAL BEHAVIOR WITH ANALYTICAL PREDICTIONS

by

J. Liu, N. Todreas

Energy Laboratory

and

Department of Nuclear Engineering

Massachusetts Institute of Technology

Cambridge, Massachusetts 02139

Topical Report for Task #3 of the
Nuclear Reactor Safety Research Program

sponsored by

New England Electric System
Northeast Utilities Service Co.

under the

MIT Energy Laboratory Electric Power Program

Energy Laboratory Report No. MIT-EL 77-009

Draft: June, 1977
Final: February, 1979

Reports Issued Under this Contract

A. Topical Reports

P. Moreno, C. Chiu, R. Bowring, E. Khan, J. Liu, N. Todreas "Methods for Steady State Thermal/Hydraulic Analysis of PWR Cores," Report MIT-EL-76-006, Rev. 1, July 1977 (Orig. 3/77).

J. Liu, N. Todreas, "Transient Thermal Analysis of PWR's by a Single Pass Procedure Using a Simplified Nodal Layout," Report MIT-EL-77-008, Rev. 1, February 1979 (Orig. 6/77).

J. Liu and N. Todreas, "The Comparison of Available Data on PWR Assembly Thermal Behavior with Analytical Predictions," Report MIT-EL-77-009, Rev. 1, February 1979 (Orig. 6/77).

B. Papers

C. Chiu, P. Moreno, R. Bowring, N. Todreas, "Enthalpy Transfer Between PWR Fuel Assemblies in Analysis by the Lumped Subchannel Model," forthcoming in Nuclear Science & Engineering.

P. Moreno, J. Liu, E. Khan, N. Todreas, "Steady State Thermal Analysis of PWR's by a Single Pass Procedure Using a Simplified Nodal Layout," Nuclear Science & Engineering, Vol. 47, 1978, pp. 35-48.

P. Moreno, J. Liu, E. Khan and N. Todreas, "Steady-State Thermal Analysis of PWR's by a Simplified Method," American Nuclear Society Transactions, Vol. 26, 1977, p. 465.

ABSTRACT

The comparison of available data with analytical predictions has been illustrated in this report.

Since few data on the cross flow are available, a study of parameters in the transverse momentum equation were performed to assess the sensitivity of results to their assumed values. It is confirmed that effects of these parameters on the overall results are not significant under PWR operating conditions.

Data on subchannel properties of quality and mass flux were also assessed. From the data comparisons, it is evident that COBRA which is the tool of the simplified method can successfully predict the PWR normal operating conditions and cannot predict the trend under bulk quality conditions ($X_e > 0.02$).

ACKNOWLEDGEMENTS

This work was initiated under the sponsorship of the Electric Power Research Institute. It was completed as part of the Nuclear Reactor Safety Research Program under the Electric Power Program sponsored by New England Electric System and Northeast Utilities Service Company.

We would like to thank the above Institute and Company for their help to make this work possible.

TABLE OF CONTENTS

Page

LIST OF TABLES

LIST OF FIGURES

LIST OF APPENDICES

CHAPTER 1

INTRODUCTION

The comparisons of the simplified method with detailed analysis were accomplished in the previous work.[1,15] It was proved that results obtained by the simplified method are close to those from other more complex methods. In order to have a satisfactory thermal hydraulic analysis method, the comparison between different methods is important but not enough. Check of the results with experimental data is equally important. The purpose of this study is to compare the physical model and certain empirical constants used in the simplified method to actual data. It should be noted that the model and constants are those of the COBRA family of codes. Chapter 2 treats the crossflow resistance parameters. Chapter 3 treats the overall two phase flow model.

Few experimental data on the crossflow resistance are available. Therefore, a study of parameters in the transverse momentum equation were performed (Chapter 2) to assess the sensitivity of results to their assumed values. Only small effects of these parameters on the overall results can be detected.

Unfortunately, only limited data on core and assembly thermal parameters have been published in the open literature.

Better understanding of the coolant physical phenomena of an actual multirod bundle which is placed in an actual reactor core is essential to assess the simplified method. Nonetheless, from the available data, it is evident that COBRA which is the tool of the simplified method can predict conditions of single phase and subcooled boiling with negative equilibrium quality ($X_e \leq 0$) satisfactorily. It can not predict the trend under bulk quality condition ($X_e > 0.02$). Even though the bulk quality seldom occurs under normal PWR operating conditions, a new physical model which can predict the trend of bulk quality flow for PWR's under severe transients is still needed.

Appendix A is the derivation of the method to simulate a channel porous blockage which was used in Chapter 2.

Appendix B presents the discussion of the cross flow resistance coefficient and the recommended value.

Chapter 2

CROSS FLOW PARAMETERS SENSITIVITY STUDY

2.1 Introduction

In COBRA IIIC,[2] the transverse momentum equation introduces two parameters: s/l and K.

where s/l is the ratio of the gap length to the transition length for the pressure, and

K is the cross flow resistance coefficient without inertial effect.

The COBRA IIIC manual notes that the effects of s/l and K on the results are negligible. This was demonstrated in the manual by examining the terms in the COBRA IIIC transverse momentum equation, and by the results of a BWR bundle sample problem as shown in Table 2.1. In order to confirm or check the above statement, analysis of a two channel geometry using the COBRA IIIC/MIT code with and without porous blockage cases, and another independent case of a six-channel geometry with inlet flow upset condition have been performed with different values of s/l and K.

The results show that the statement that the effects of the two parameters on the results are negligible is generally correct if by results we consider only the sub-channel exit enthalpy. The reasons are:

(1) Under normal operating conditions, the transverse momentum equation does not play very important role.

(2) For economic reasons, a comparatively large axial step length is usually used.

(3) Total cross flow is small even when there is a large local change.

(4) The power difference between channels is not large enough.

The statement that the precise values of s/l and K are not necessary is not correct if we consider results for local cross flow. Specifically,

(1) The effects of s/l and K on the local cross flow under the inlet flow upset and the porous blockage conditions are large.

(2) The location of MDNBR may change due to the large local change of cross flow.

Nine cases were examined in this study. They represent combinations of three different values of both s/l and K under four different conditions. The values of s/l and K, as well as the assigned case number are shown in Table 2.2. The four different conditions and the number of channels analyzed under each condition are summarized in Table 2.3.

The method to simulate a channel porous blockage using different values of the spacer loss coefficient is discussed in Appendix A.

The realistic range of K was analyzed in Appendix B.

The nominally correct value of s/l was derived in Reference 3.

2.2 Cases with Inlet Flow Upset

A series of cases of two connected bundles with inlet flow upset and zero power conditions were performed. Figure 2.1 illustrates the geometry of thse two bundles and the location of the three spacers. The ratio of high mass flow rate m_I to the low mass flow rate m_{II} of 0.75 was selected for the analysis. The two bundles have been divided into six subchannel regions radially and seventy-two slices axially to ensure a detailed analysis.

The most significant difference due to different values of s/l and K under this condition is the diversion cross flow between subchannels. The six subchannel model was divided in such a way that the boundary between subchannels 3 and 4 is the actual boundary between the two bundles.

(See Figure 2.1). Therefore, examination of the analysis results was focused on the cross flow between subchannel's 3 and 4 and these cross flow for nine cases were plotted on Figure's 2.2 through 2.7. The nine cases were obtained by the different combinations of different values of s/l and K as shown in Table 2.2.

The effect of s/l on the cross flow between channel's 3 and 4 along the axial direction for fixed K can be seen from Figure's 2.2 through 2.4. Three values of K (0.0001, 0.5, 5.0), and three values of s/l (100., 1.3, 0.3) were tested and are indicated on the plot. The effect of s/l is to vary the inertia of the cross flow. For larger values of s/l, the inertia of the cross flow is small (see cases with s/l = 100.) or vice versa (see cases with s/l = 0.3). By this we mean that cross flow (with s/l = 100.) changes quicker than those with s/l = 0.3. It seems that the effect of s/l on the local cross flow is independent from different values of K.

The effect of K on the cross flow from subchannel 3 to subchannel 4 along the axial direction for fixed s/l can be examined from Figure's 2.5, 2.6. The effect of K is not to vary the inertia but the magnitude of the cross flow. If larger values of K (e.g. K = 5.) are used, smaller magnitude of cross flow will be generated, or vice versa

(e.g. K = 0.0001). The effect of K becomes insignificant for smaller values of s/l. For example the differences of cross flow within Case's 3, 6, and 9 (s/l = 0.3 for all three cases) due to different values of K (ranging from 0.0001 to 5.0) is hard to detect. So there is no comparision plot of these three cases.

From Figure's 2.2 through 2.6, it is clear that the cross flow pattern along the channel varies a lot due to the effects of s/l and K as shown again in Figure 2.7 for extreme Case's 1, 5 and 9.

For fixed s/l and K (i.e. for fixed case), the five cross flow patterns along the axial direction between all six subchannels are all alike. This is not surprising, since only one set of values of s/l and K was inputed to the computer code for the five subchannel boundaries. Because of this similar cross flow pattern, the axial mass flow rate of a certain channel does not change as dramatically as the cross flow due to different values of s/l and K. Also, the axial mass flow rate is more important than the cross flow in determining the overall results.

The small difference of channel axial mass flow rate between cases was examined and confirmed by an example. Refere to Figure 2.8, the difference of axial mass flow rate between Case's 1 and 9 for channel 4 was calcu-

lated and compared as follows:

The difference between Case's 1 and 9 of cross flow through channel's 3 and 4 integrated from inlet to the exit is +15%. The difference between the same two cases of cross flow through channel's 4 and 5 is +15.5%. Due to the compensation of differences, the exit mass flow rate of channel 4 has only 0.5% difference between these two cases.

Therefore, the effects of s/l and K on the overall results are not significant even though the effects on cross flow are significant under the inlet flow upset condition.

2.3 Cases of Channel with Porous Blockage

In order to have a situation such that the transverse momentum equation plays more important role than under normal operating condition, a porous blockage with a loss coefficient of 25. was installed at the mid position in one of the two channels. The blockage was simulated in terms of the spacer loss coefficient which is an input parameter to COBRA IIIC code. Details of this simulation are discussed in Appendix A.

Equal channel power input was used to ensure that the cross flow generated could be subscribed to the porous

blockage condition.

The diversion cross flows at the location just after the blockage for different values of s/l and K are shown in Figure 2.9. From this figure, it is clear that the effect of s/l on the local cross flow will increase as the value of K decreases. Generally, s/l and K both have the same order of magnitude effect on the local cross flow. Note that unrealistic values of K and s/l were selected in order to investigate the effect of K and s/l under extreme conditions. Realistic ranges of K and s/l were investigated and discussed in Appendix B and Reference 3 respectively.

The cross flow patterns along the axial direction for nine different cases were plotted in Figures 2.10, 2.11 and 2.12. The location of the porous channel blockage was indicated at 10.5 inches from the inlet. Also the value of hydraulic diameter was indicated as D_h on each figure. By comparing these three figures, two important observations can be made. First, the effect of s/l on the cross flow pattern is to vary the inertia of the cross flow. Second, the effect of K on the cross flow pattern is to vary the magnitude of the cross flow. Additionally, the effect of K is insignificant as the value of s/l becoming smaller. The figures also indicate that

even though the local cross flow at the location just after the blockage changes considerably from case to case, the magnitude of the total cross flow which is the area under the curve is very similar. The difference of the total cross flow for two extreme cases (Case's 1 and 9) analyzed is only 3%.

Results of enthaply and MDNBR at the location just after the blockage for different cases are listed in Table's 2.4 and 2.5 respectively. Since these are a secondary effect of the transverse momentum equation, the differences are small.

The difference of the MDNBR for two extreme cases is the same order of magnitude as the total cross flow (i.e. 3.4%). Since MDNBR varies linearly with axial flowrate which for this two channel case varies linearly with total cross flow. Since the channels have equal power, the difference of the exit enthalpy for two extreme cases is even smaller (0.2% only) than those which have different power.

2.4 Cases of Channel with Power Upset

A power ratio of 1.8 : 0.2 was selected to characterize a power upset situation of the two-channel analysis. No spacer was installed in order to examine the effects of

s/l and K on the results of a pure power upset condition.

The magnitude of cross flow for the nine cases is only in the order of 10^{-3}lbm/sec ft. The maximum differences of local cross flow between nine cases are shown in Table 2.6. The differences are very small. From this result, no effect of K on cross flow can be detected for the same value of s/l. The effect of s/l on cross flow is a little more significant than the effect of K.

The hot channel exit enthalpy for the nine different cases are all the same. Because of the same value of exit enthalpy, the same value of MDNBR was generated by the nine different cases.

The conclusion of this analysis is that the effects of the parameters of s/l and K is positively negligible for this pure power upset condition.

2.5 Realistic Cases

A power ratio of 1.2 : 0.8 and a spacer loss coefficient (K_G) of 5. are quite realistic for an ordinary reactor bundle. Based on the above data, analysis was performed to examine the different results due to different values of s/l and K.

The effects of s/l and K on the cross flow pattern along the axial direction are quite similar to the cases

of channel with porous blockage as mentioned in section 2.3. Results of the local cross flow at location just after the spacer are shown in Table 2.7. It can be seen that effects of s/l and K on the local cross flow do have the same order of magnitude.

The nine different values of hot channel exit enthalpy and MDNBR are listed in Table's 2.8 and 2.9 respectively. Although the differences are detectable, the differences are insignificant.

Therefore, for a realistic bundle condition, the sensitivity to the parameters of s/l and K on the overall results is not significant. Only the location of MDNBR along the axial direction may change from case to case.

2.6 Various Conditions for the Recommended Values of K and s/l

Recommended values of 0.27 and 0.9187 for K and s/l respectively were utilized to analyze the various conditions mentioned in Section's 2.3, 2.4, and 2.5.

Figure 2.13 shows the cross flow pattern along the axial direction for the porous blockage condition (i.e. K_G = 25., equal power, equal inlet flows). The hot channel enthalpy and DNBR just after the porous blockage is 556.34 Btu/lb and 4.506 respectively.

For the power upset condition, (i.e. K_G = 0., power ratio = 1.8 : 0.2, equal inlet flow) cross flow is in a small order of magnitude. The hot channel exit enthalpy and MDNBR is 571.6 Btu/lb and 3.548 respectively.

For the realistic condition, (i.e. K_G = 5., power ratio = 1.2 : 0.8, equal inlet flow) hot channel exit enthalpy of 568.75 Btu/lb and MDNBR of 4.545 were observed.

Comparing all the above results with the results obtained in the previous sections, only very small differences except for local cross flow can be noticed. This says that better values of s/l and K are not necessary for a better overall result except for local cross flow.

2.7 Effect of Axial Step Length

The flow disturbance due to a porous channel blockage can be detected within a small range around the blockage. This small disturbed flow region, for this degree of blockage studied here, is roughly the same order of magnitude as the channel hydraulic diameter. Therefore, for larger axial step length, the effect on the flow of a porous blockage is small. The sensitivity to s/l and K under blockage conditions with large axial step length is also small. This can be demonstrated by a case which has the same input parameters as used in Section 2.3 but a larger

axial step length. It was accomplished by selecting a longer channel (126.7 in) with the same number of axial nodal points.

The results of cross flow at the location just after the blockage as functions of s/l and K were plotted in Figure 2.14. Comparing Figure 2.14 with Figure 2.9, it is very clear that the sensitivity to s/l and K is smaller for larger axial step length.

Under this condition, the differences of enthalpy, MDNBR between cases with different s/l and K are even smaller. For example, a typical result of MDNBR along the hot channel for two different values of s/l is shown in Table 2.10.

Also cases which have different power input with and without porous channel blockage under large axial step length condition have been analyzed. For a spacer loss coefficient K_G = 5 blockage channel, the results of the local cross flow are shown in Table 2.11. The power ratio (1.5) was also taken as 1.2 : 0.8. The exit enthapy of hot channel for this case is shown in Table 2.12. It shows that even the case has different power ratio along with a blockage (K_G = 5) located in one of the two channels, the effect of s/l on the overall result is small.

The power input ratio was increased to 9 (1.8 : 0.2),

there is still no change of the exit enthalpy difference as shown in Table 2.13. Therefore, for larger axial step length model, the effects of s/l and K are hard to detect.

This can also be explained by inspecting the finite difference form of the combined transverse momentum equation: (2)

$$m = \frac{1}{\Delta t} + \frac{u^*}{\Delta x} + \left(\frac{s}{l}\right)C + \left(\frac{s}{l}\right)\frac{2u^*}{A}\Delta x$$

where u* is the average of the two subchannel velocities. The relative importance of the terms can be controlled by arbitrarily selecting the axial step lenth Δx. For larger value of Δx, the last term is the largest one. The parameter K is contained in the third term. Since this term is small, the effect of K is small. Since the last term contains both Δx, and s/l the effect of s/l is small for larger Δx.

Parameter Sensitivity Evaluation for BWR Bundle Sample Problem

Parameter	Pressure Ahead of Blockage (psia)	G Minimum (10^6 lb/hr ft^2)	Enthalpy 1 ft Downstream of Blockage (Btu/lb)
No Blockage	3.50	.958	657.72
Base Case Blockage	3.97	.380	667.70
$\kappa_{ij} = 1.0$	3.98	.381	667.67
$K_{ij} = 0.25$	3.97	.380	667.74
$s/\ell = 1.0$	3.96	.373	667.38
$s/\ell = 0.25$	3.99	.390	668.31
$\Delta x = 4$ inches	--	.384	669.92
$u^* = \begin{cases} u_{ij}; & w_{ij} > 0 \\ u_{ij}; & w_{ij} \leq 0 \end{cases}$	3.97	.423	665.90
$u^* = \min(u_i, u_j)$	3.98	.423	668.76

Table 2.1 (From Table 2 of Ref. 2)

K \ s/l	100	1.3	0.3
.0001	Case 1	Case 2	Case 3
0.5	Case 4	Case 5	Case 6
5	Case 7	Case 8	Case 9

Table 2.2

Nine Cases Analyzed in This Study

Conditions	No. of Channels
<u>Inlet Flow Upset</u> $\frac{\text{Hight Mass Flow Rate}}{\text{Low Mass Flow Rate}} = 0.75$	6
<u>Porous Blockage</u> Loss Coefficent $K_G = 25.$	2
<u>Power Upset</u> $\frac{\text{High Power}}{\text{Lower Power}} = \frac{1.8}{0.2}$	2
<u>Realistic</u> Power Ratio: 1.2 : 0.8 Loss Coefficient: $K_G = 5.$	2

Table 2.3 Four Conditions Analyzed in This Study

K \ s/l	100	1.3	0.3
0.0001	556.28	556.31	556.38
0.5	556.33	556.35	556.42
5.0	556.6	556.61	556.67

Channel with Blockage

K \ s/l	100	1.3	0.3
0.0001	556.26	556.24	556.18
0.5	556.22	556.2	556.16
5.0	556.09	556.08	556.06

Channel without Blockage

Table 2.4 Enthalpy (Btu/lb) at Location 1.04 D_h after Porous Blockage (K_G = 25)

K \ s/l	100	1.3	0.3
0.0001	4.467	4.496	4.564
0.5	4.467	4.492	4.560
5.0	4.472	4.488	4.522

Table 2.5 MDNBR at Location 1.04 D_h After Porous Blockage (K_G = 25)

K \ s/l	100	1.3	0.3
0.0001	3.07	3.09	3.14
0.5	3.07	3.09	3.14
5	3.07	3.09	3.14

Table 2.6 Local Cross Flow (10^{-3} lb/sec ft) for Power Upset Condition

K \ s/l	100	1.3	0.3
.0001	3.822	3.515	2.886
0.5	3.538	3.305	2.781
5	2.474	2.404	2.208

Table 2.7 Local Cross Flow (lb/sec ft) after the Spacer for a Realistic Condition

K \ s/l	100	1.3	0.3
0.0001	568.52	568.7	569.6
0.5	588.52	568.69	569.04
5	568.58	568.71	568.07

Table 2.8 Hot Channel Exit Enthalpy (Btu/lb) for a Realistic Condition

K \ s/l	100	1.3	0.3
0.0001	4 585	4.556	4.472
0.5	4.586	4.559	4.478
5	4.590	4.572	4.510

Table 2.9 MDNBR for a Realistic Condition

Distance	s/l = 0.3 MDNBR	s/l = 1.3 MDNBR	
0.0	0.0	0.0	
6.0	0.0	0.0	
12.1	7.289	7.289	
18.1	7.166	7.166	
24.1	7.044	7.044	
30.2	6.922	6.922	
36.2	6.801	6.801	
42.2	6.680	6.680	
48.3	6.559	6.559	
54.3	6.439	6.439	
60.3	6.297	6.309	
66.4	4.082	4.079	Location of Porous Blockage (K_G = 25.)
72.4	4.177	4.185	
78.4	4.311	4.320	
84.5	4.428	4.435	
90.5	4.517	4.523	
96.5	4.578	4.584	
102.6	4.616	4.620	
108.6	4.631	4.635	
114.6	4.628	4.631	
120.7	4.609	4.611	
126.7	4.575	4.578	

Table 2.10 Axial Distribution of MDNBR for Constant Cross Flow Resistance K = 0.5

s/l	0.3	0.9	1.3
W_{ij}	.59395	.59806	.59865

Table 2.11 Local Cross Flow (lb/ft sec.) at Location 6.70 D_h after Blockage for Cases K_G = 5., Power Ratio = 1.2 : 0.8, and Cross Flow Resistance K = 0.5.

s/l	0.3	0.9	1.3
Exit Enthalpy (Hot Channel)	642.06	642.05	642.05

Table 2.12 Exit Enthalpy (Btu/lb) at Location 6.70 D_h after Porous Blockage for Cases K_G = 5., Cross Flow Resistance K=0.5, Power Ratio = 1.2: 0.8,

s/l	0.3	0.9	1.3
Exit Enthalpy (Hot Channel)	652.52	652.52	652.52

Table 2.13 Exit Enthalpy (Btu/lb) for Cases Power Ratio = 1.8:0.2, Cross Flow Resistance K = 0.5, No Blockage.

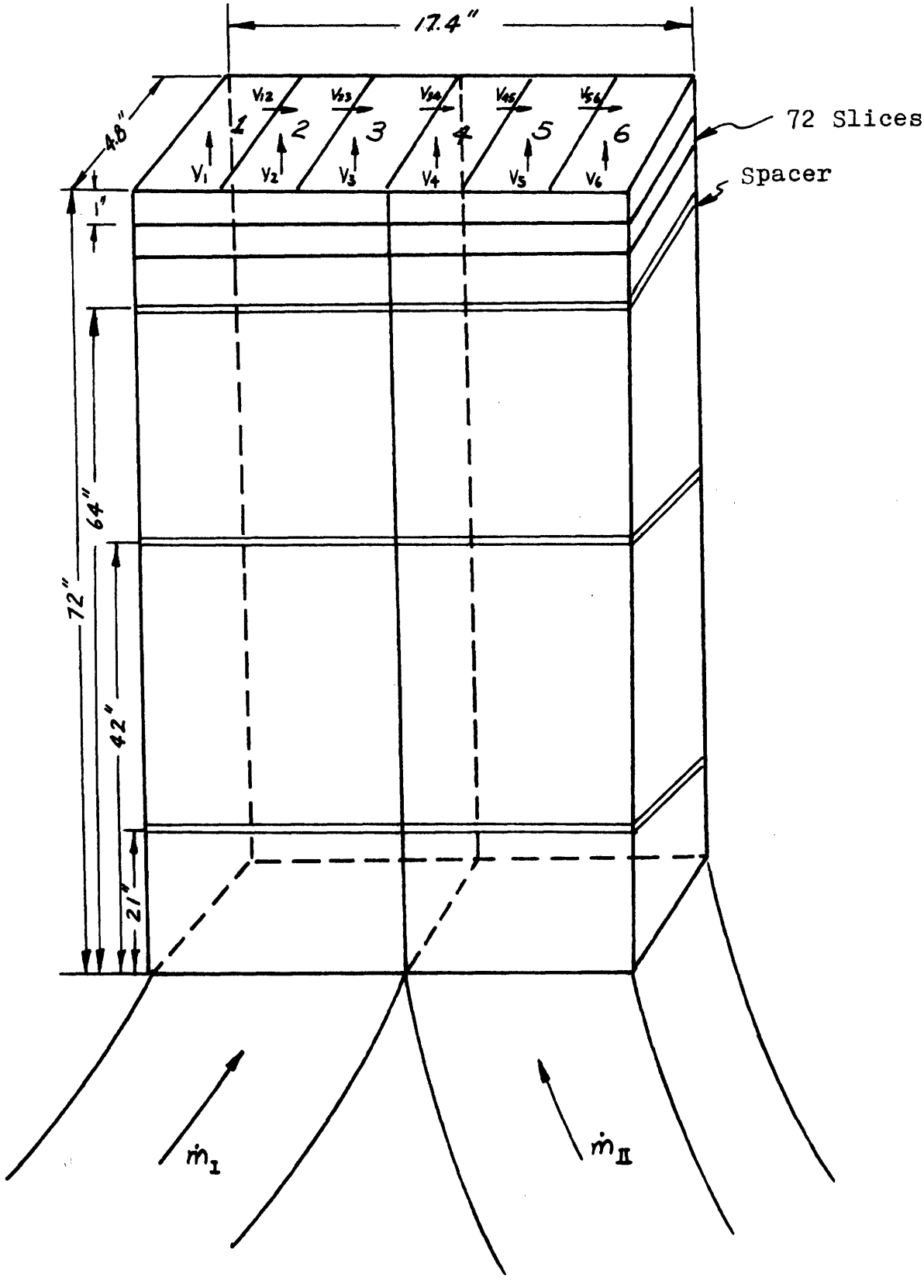

Figure 2.1 Bundle Geometry of Inlet Flow Upset Case

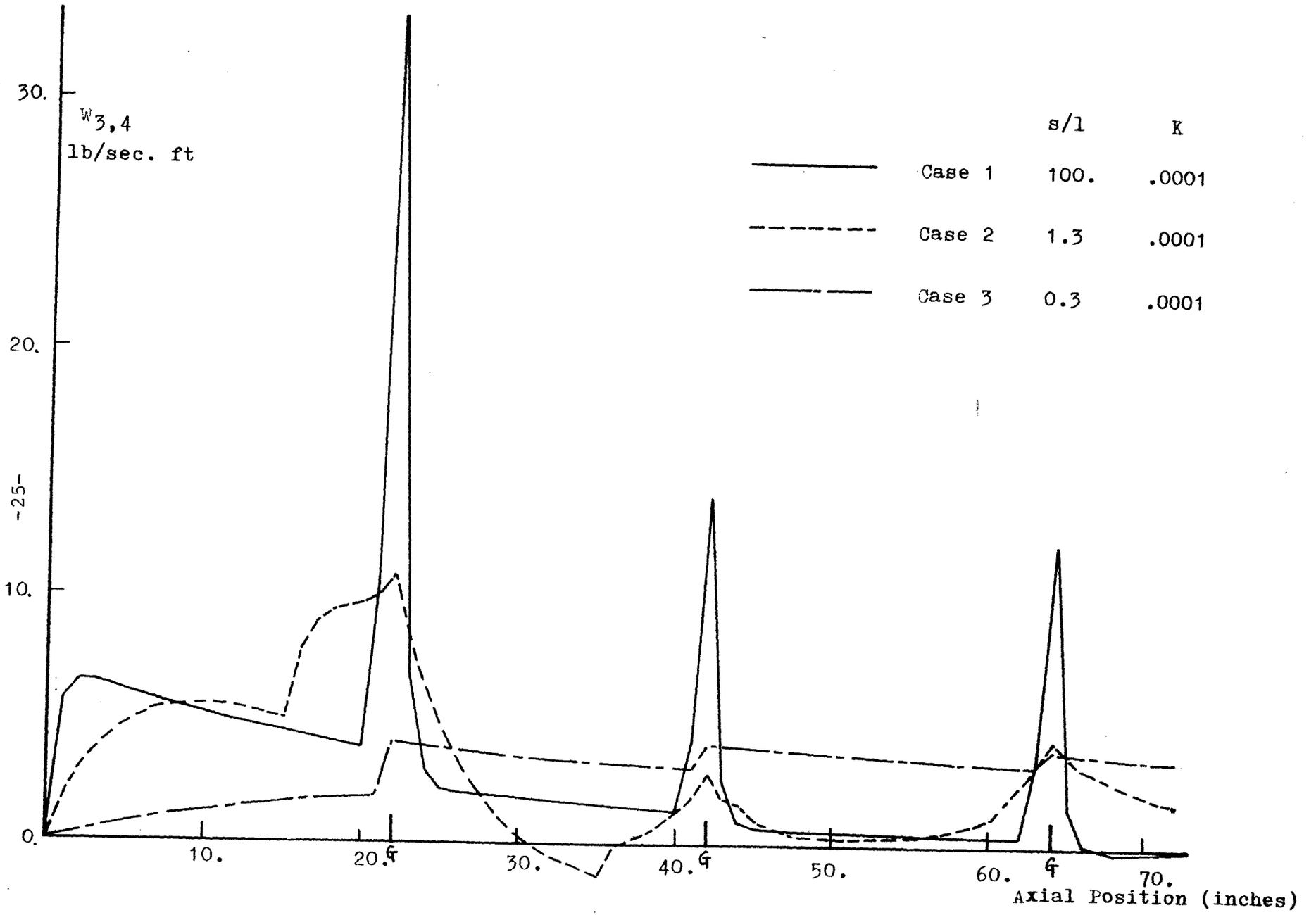

Figure 2.2 Effect of s/ℓ on Cross Flow Pattern for Inlet Flow Upset Condition

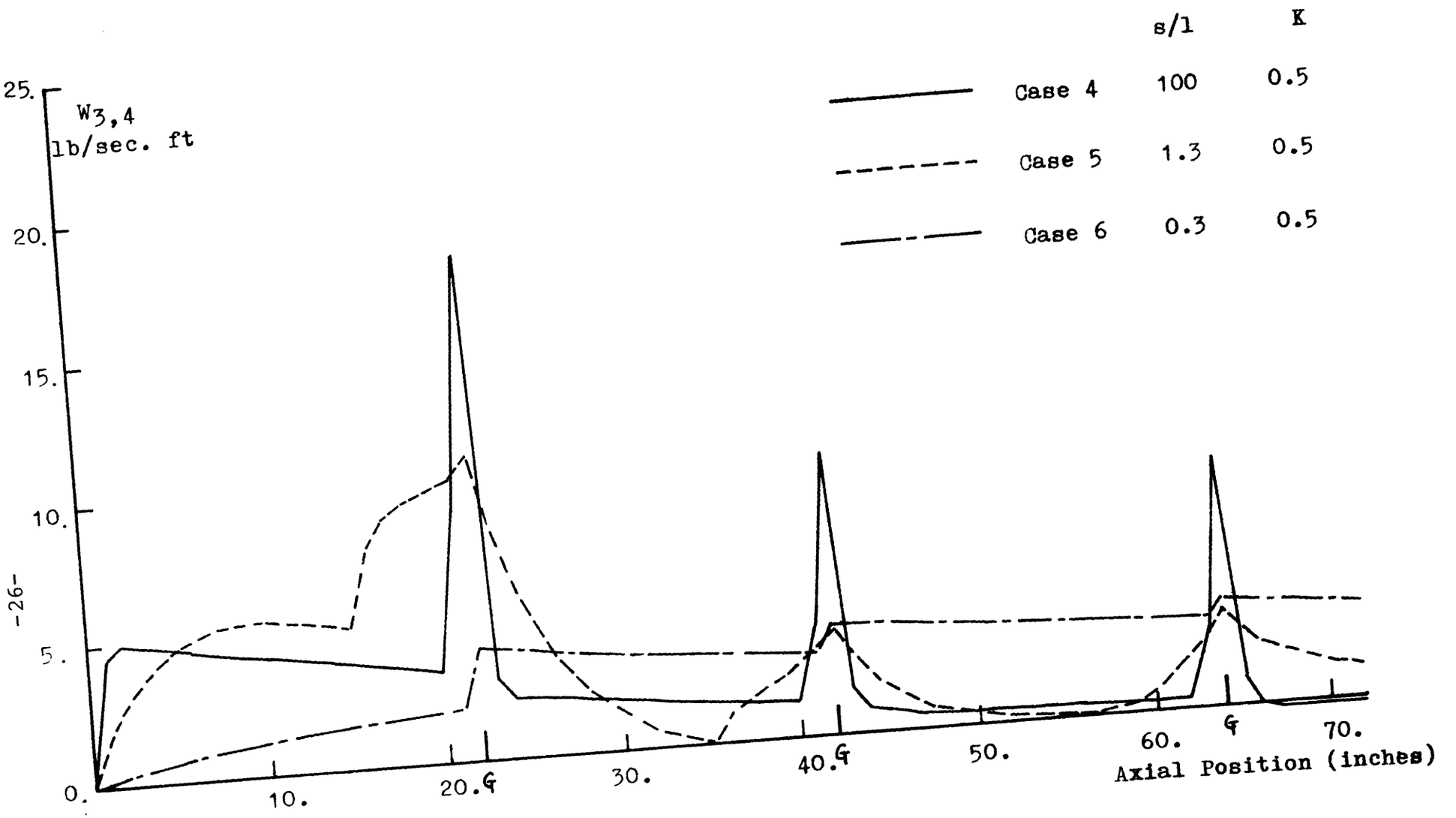

Figure 2.3 Effect of s/l on Cross Flow Pattern for Inlet Flow Upset Condition

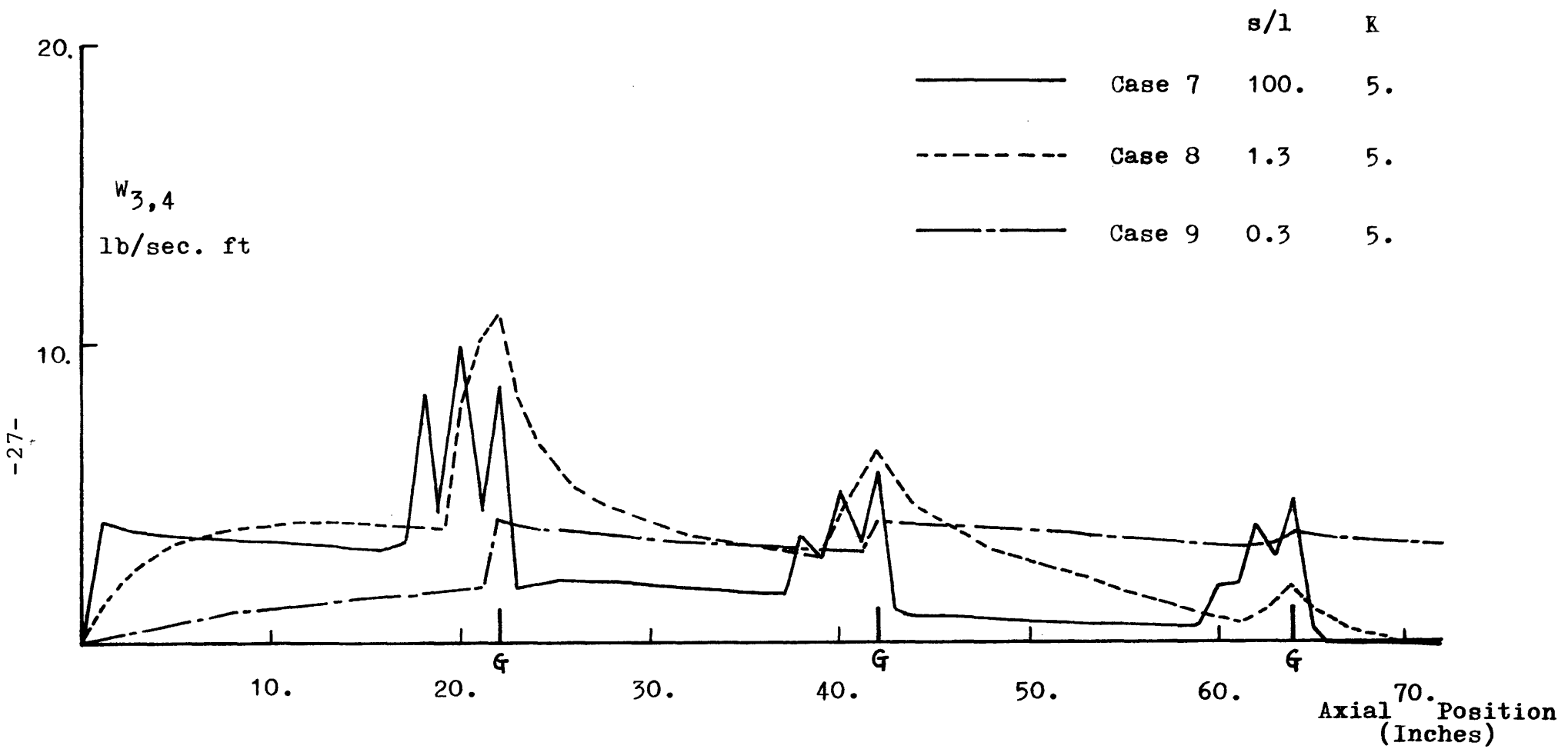

Figure 2.4 Effect of s/l on Cross Flow Pattern for Inlet Flow Upset Condition

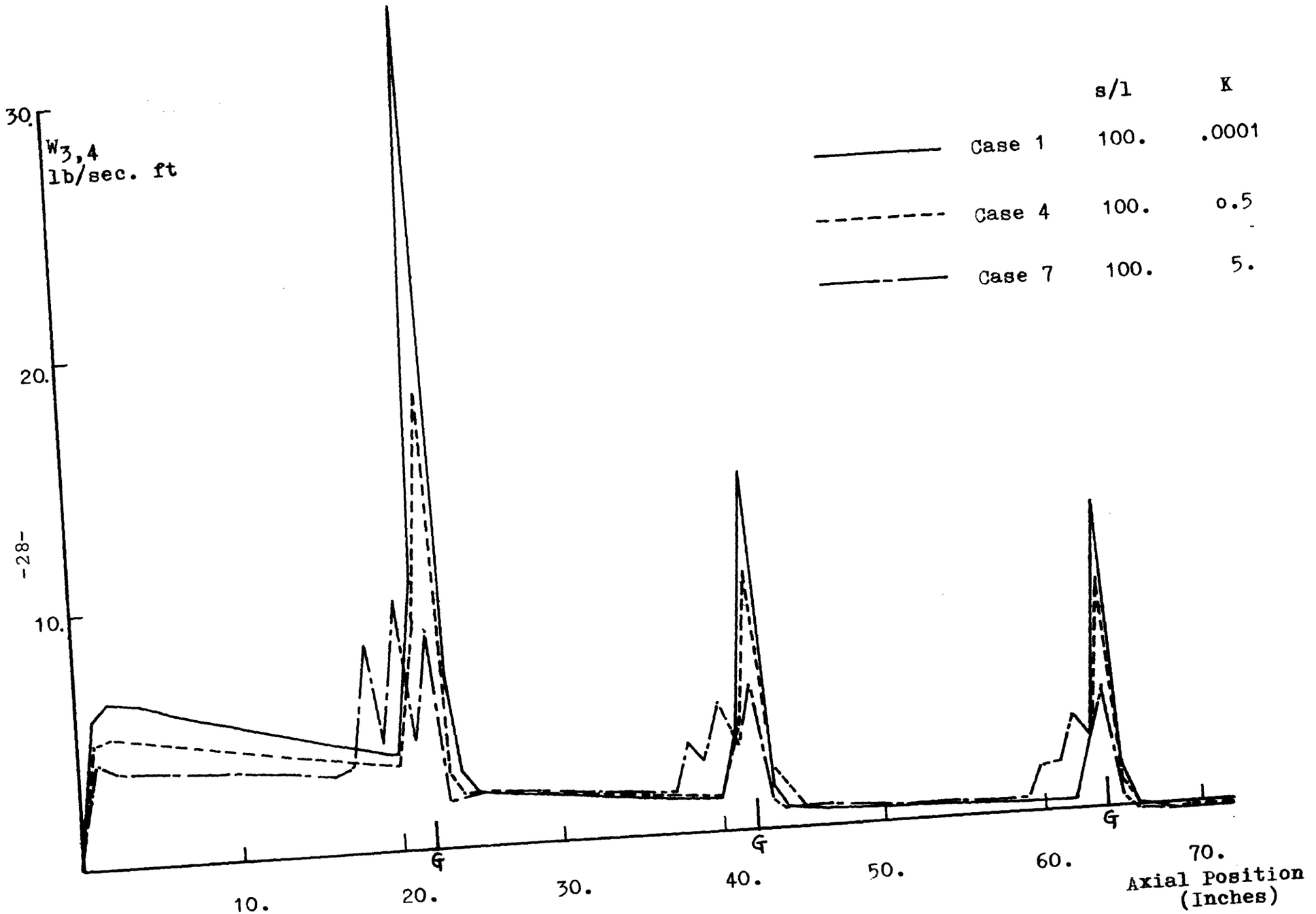

Figure 2.5 Effect of K on Cross Flow Pattern for Inlet Flow Upset Condition

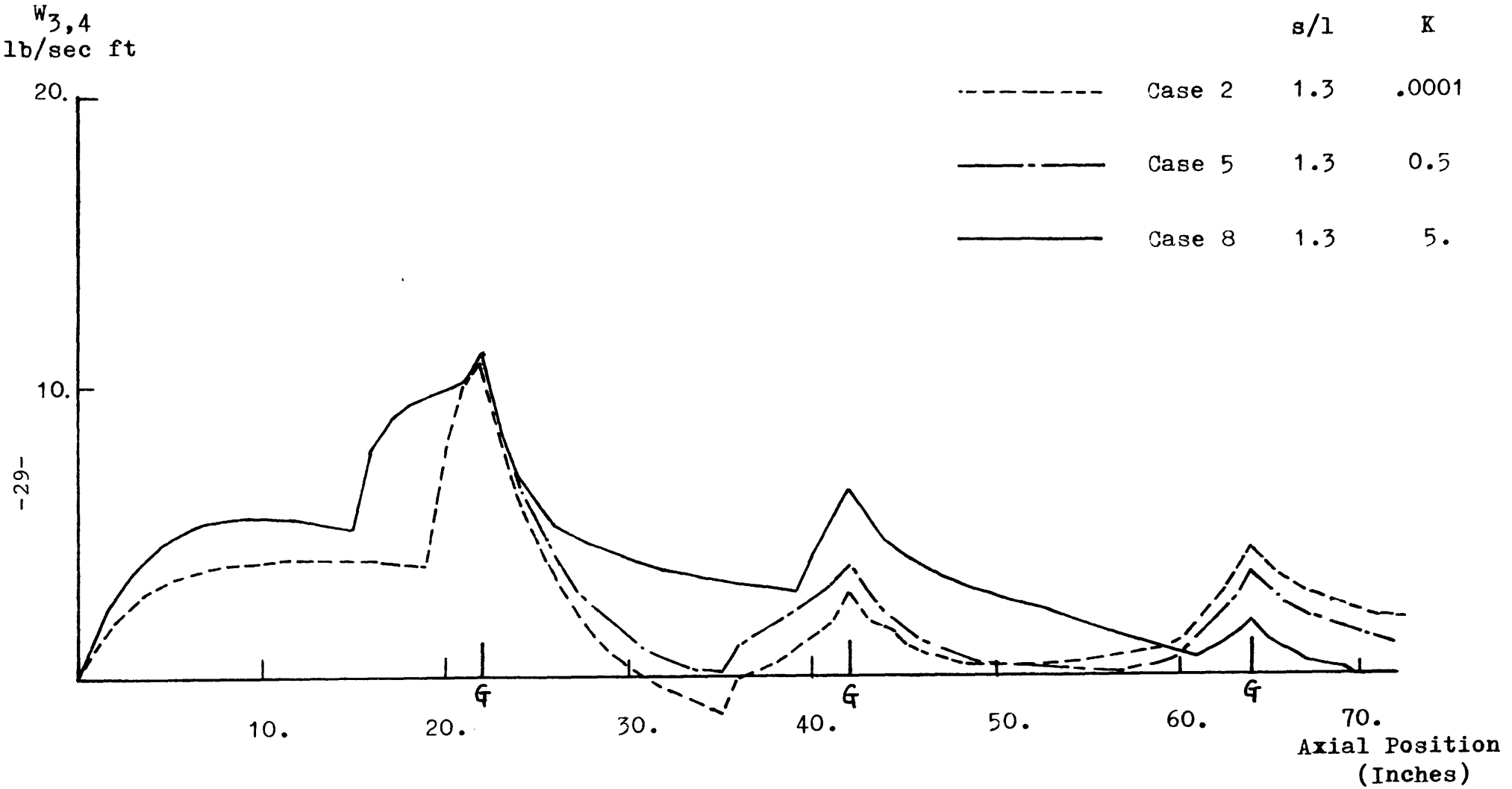

Figure 2.6 Effect of K on Cross Flow Pattern for Inlet Flow Upset Condition

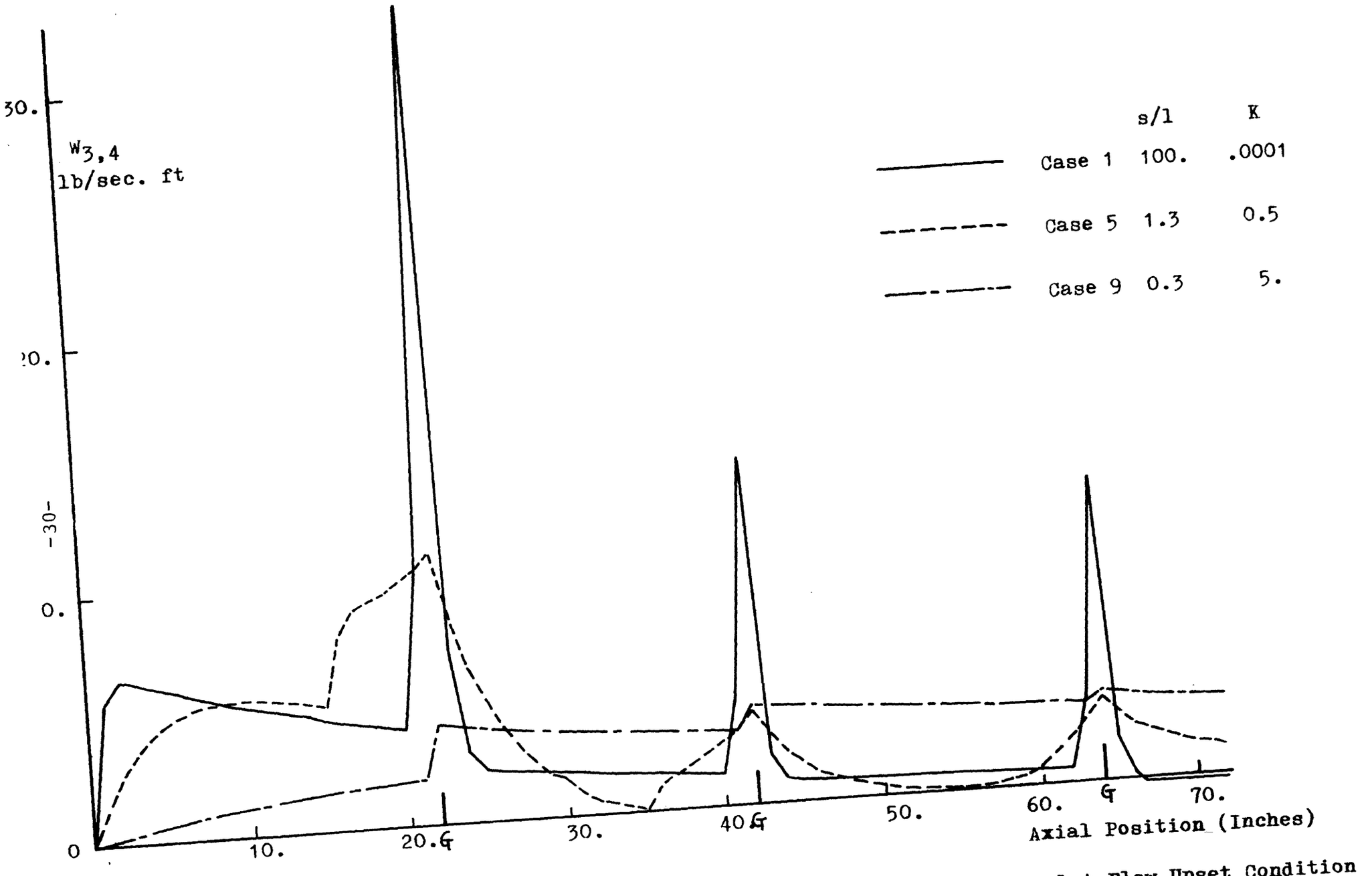

Figure 2.7 Effects of s/l and K on Cross Flow Pattern for Inlet Flow Upset Condition

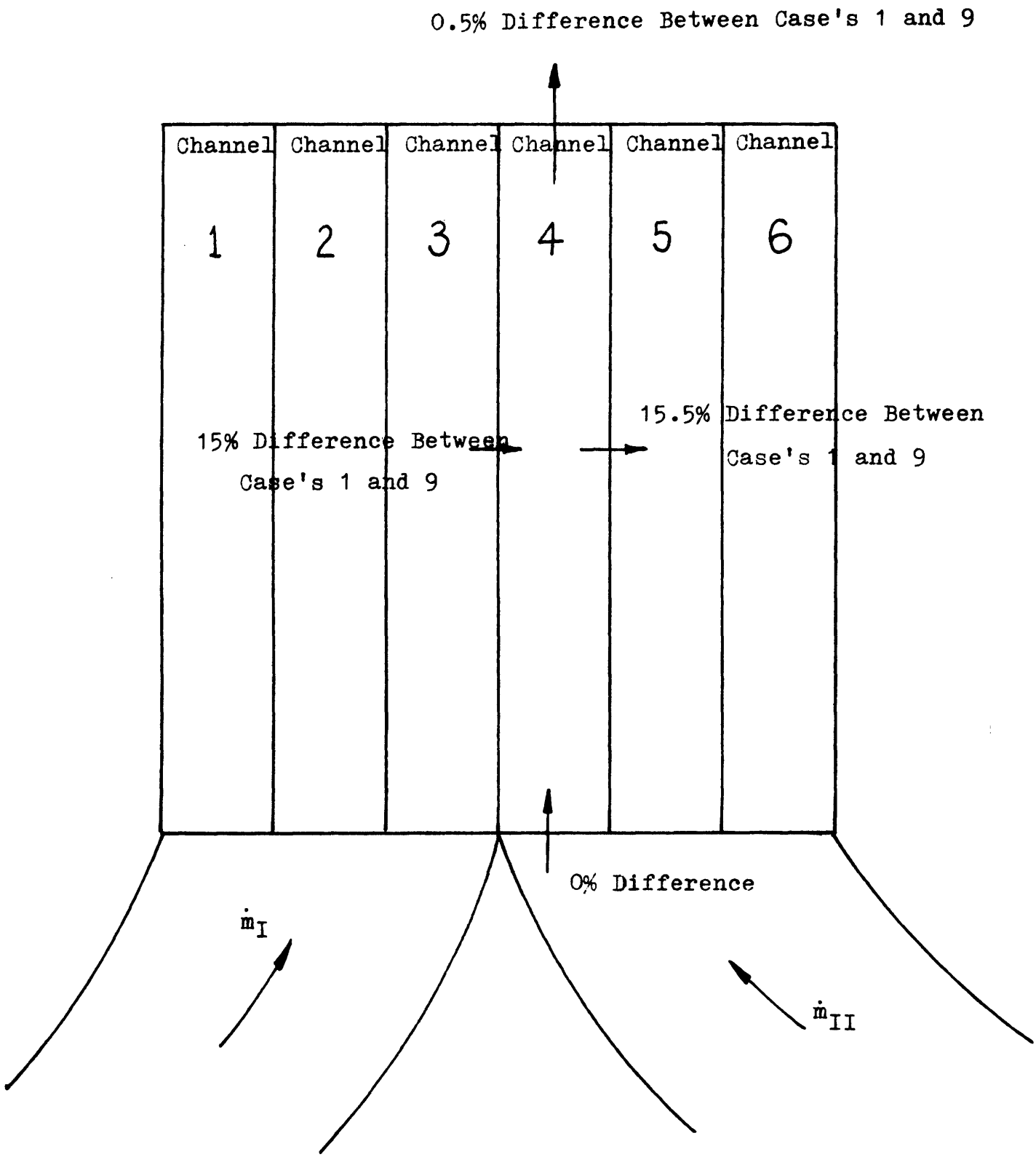

Figure 2.8 Calculation of Channel 4 exit Mass Flow Rate Difference Between Case's 1 and 9 for Inlet Flow Upset Condition

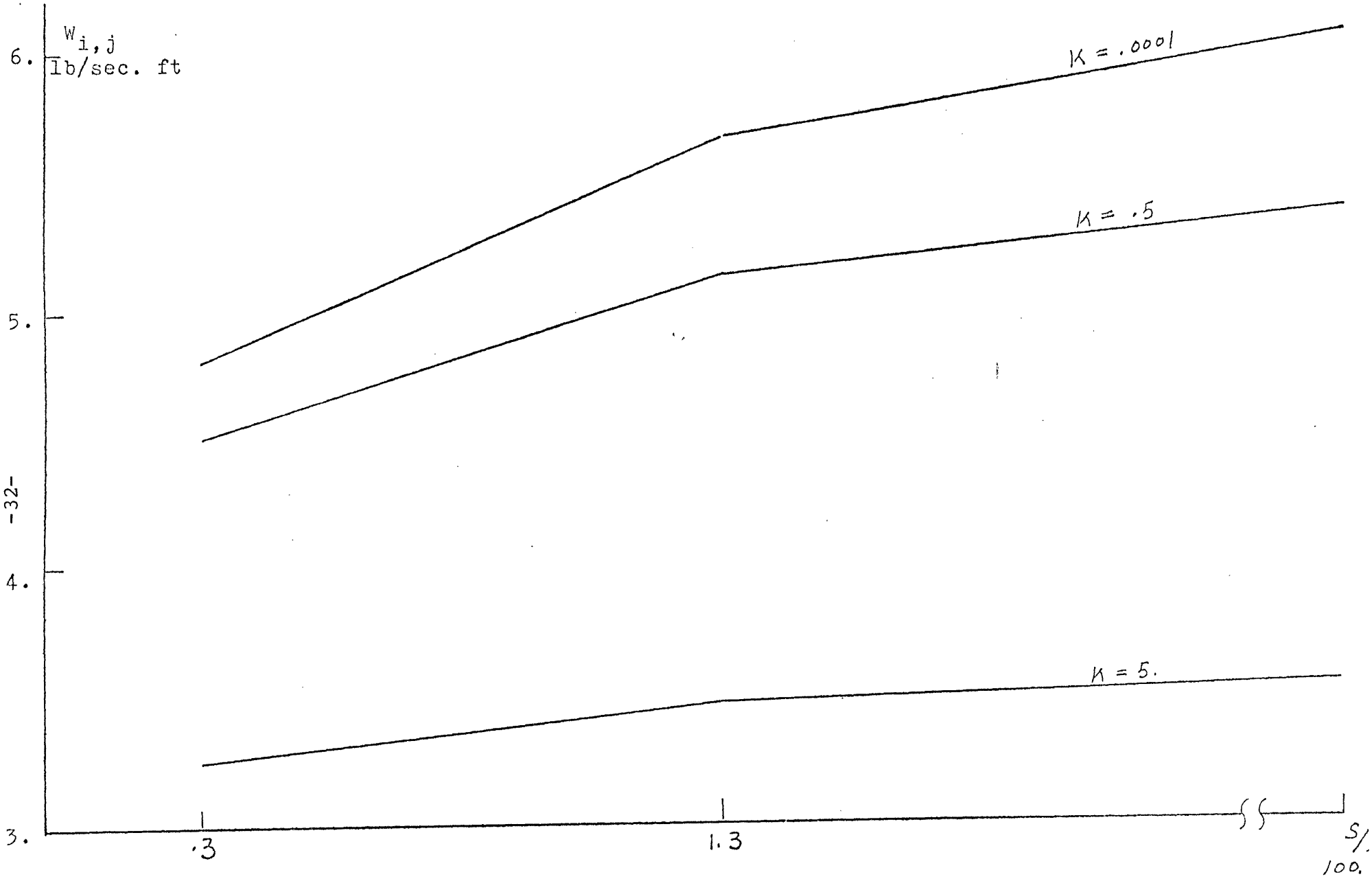

Figure 2.9 Effect of s/l and K on Local Cross Flow for Porous Blockage Condition

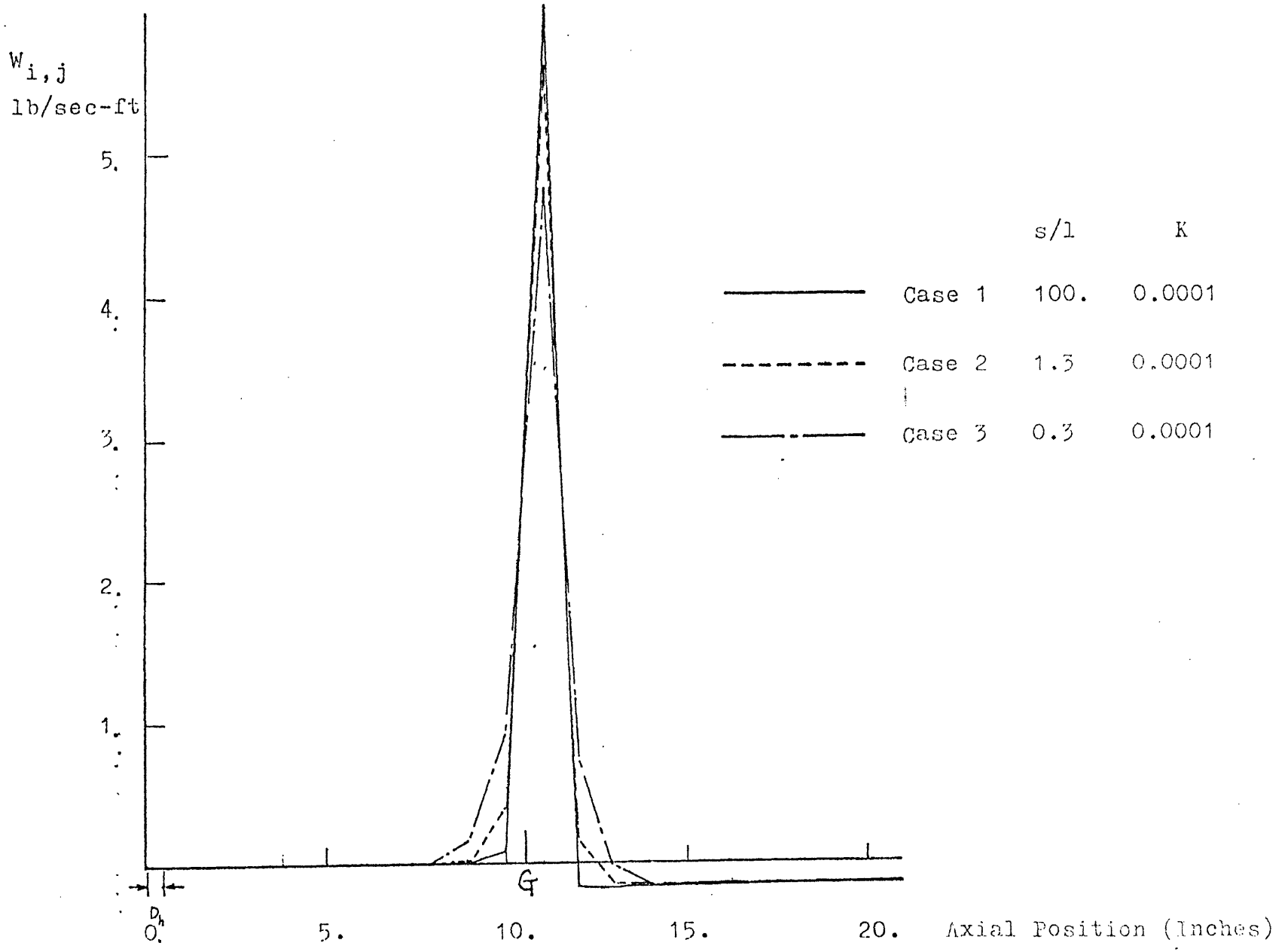

Figure 2.10 Effect of s/l on Cross Flow for Porous Blockage Condition

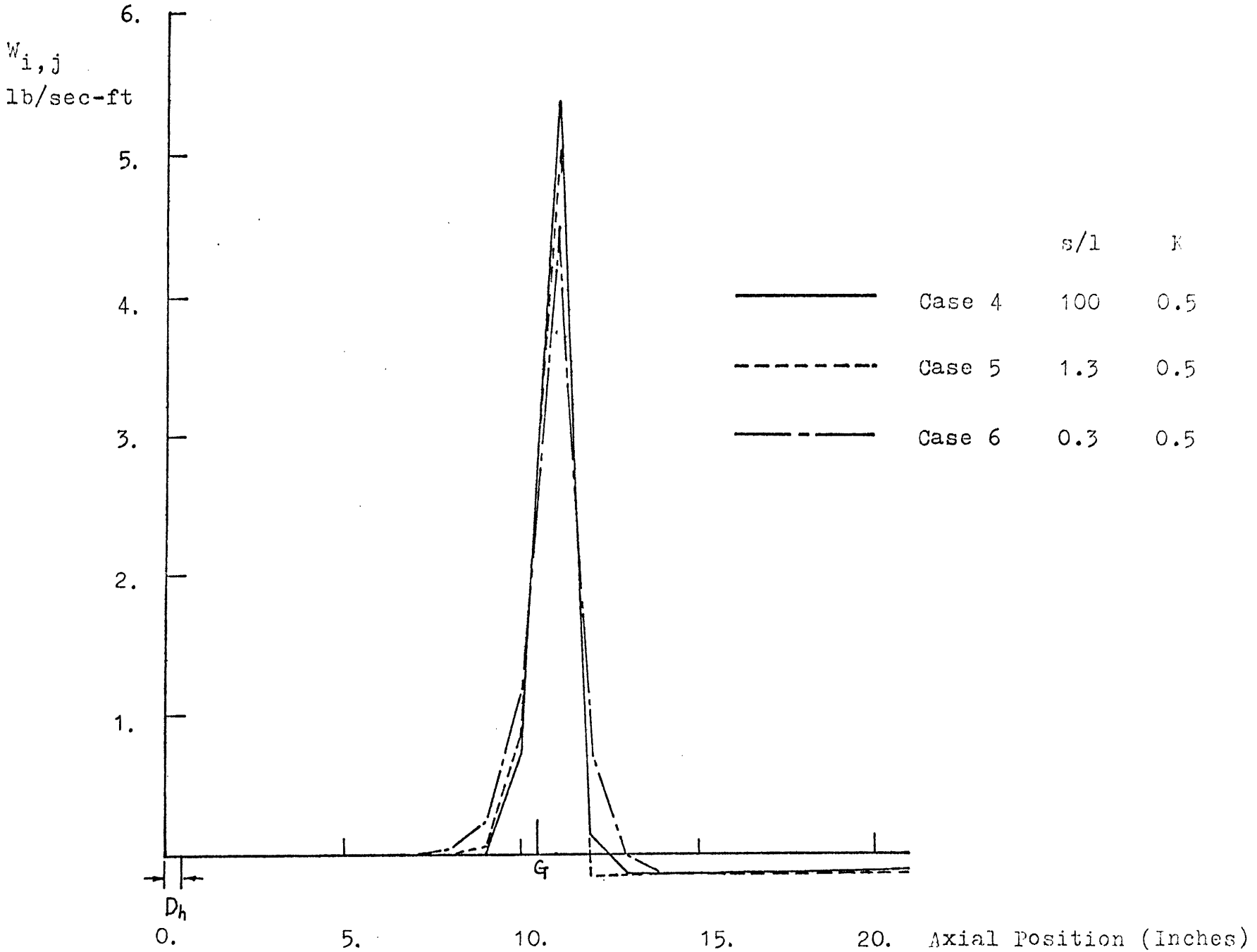

Fig 2.11 Effect of s/l on Cross Flow for Porous Blockage Condition

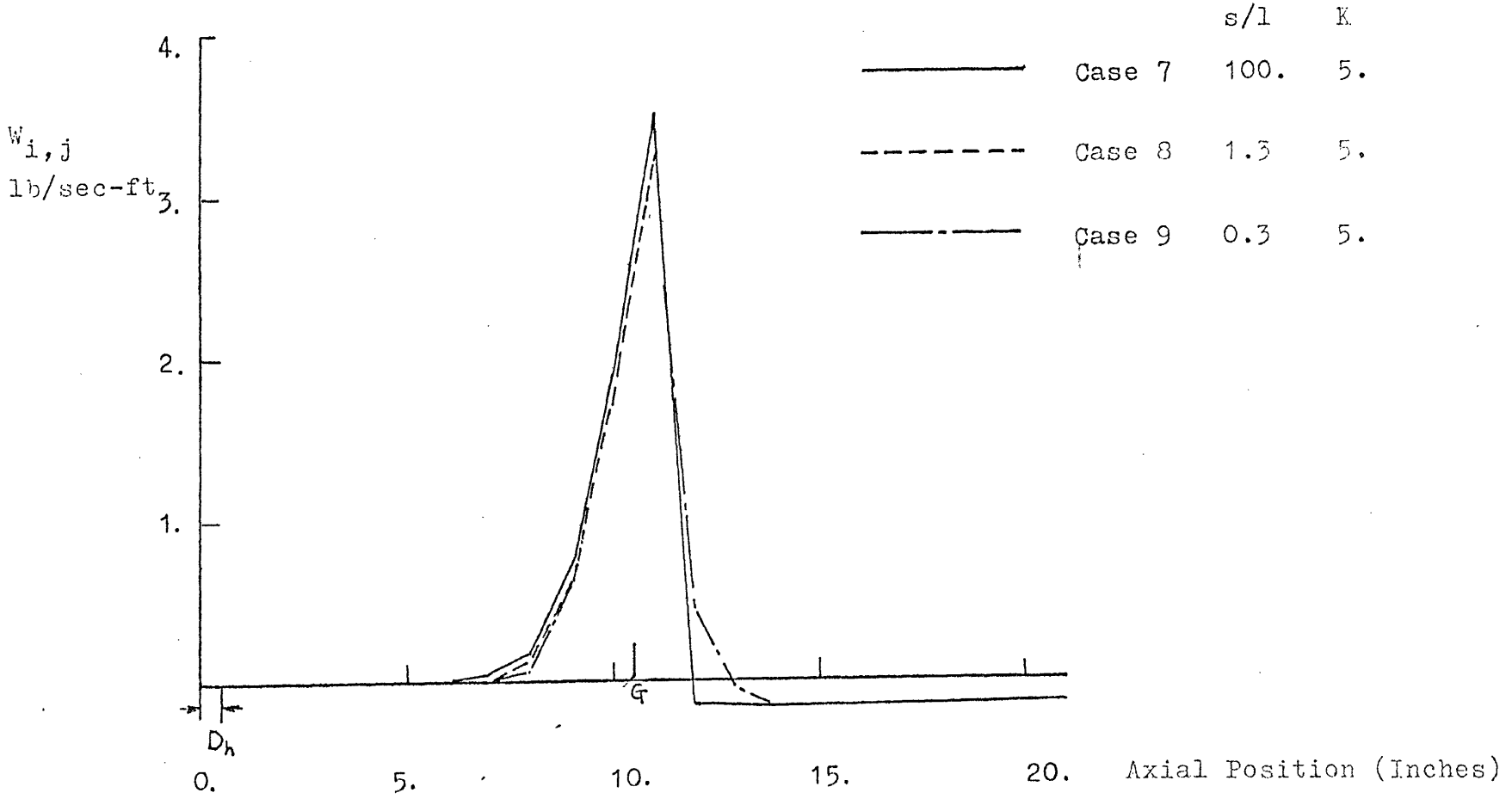

Figure 2.12 Effect of s/l on Cross Flow for Porous Blockage Condition

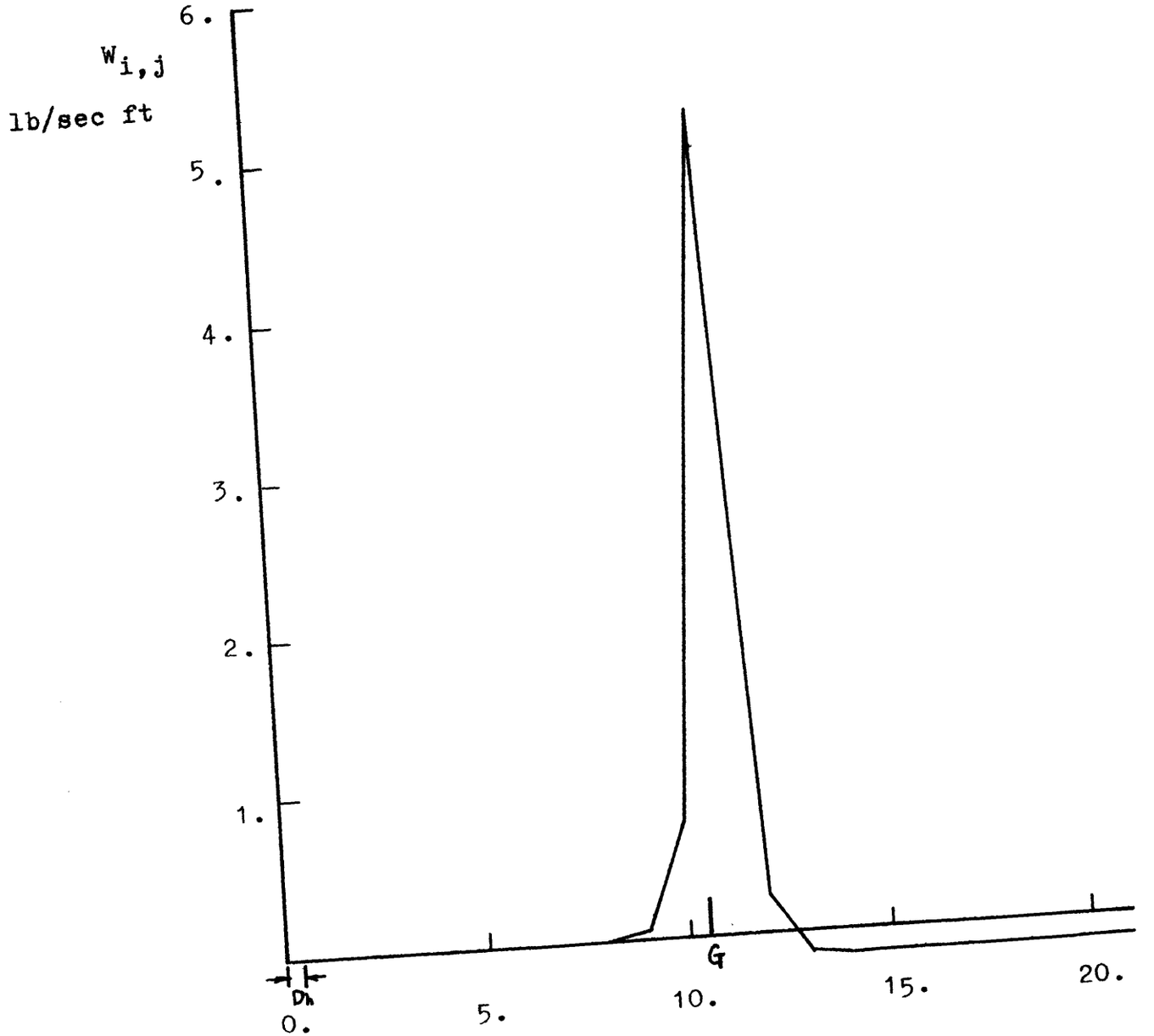

Fig 2.13 Cross Flow Pattern Generated by Using the Recommended Values of s/l and K for Porous Blockage Condition

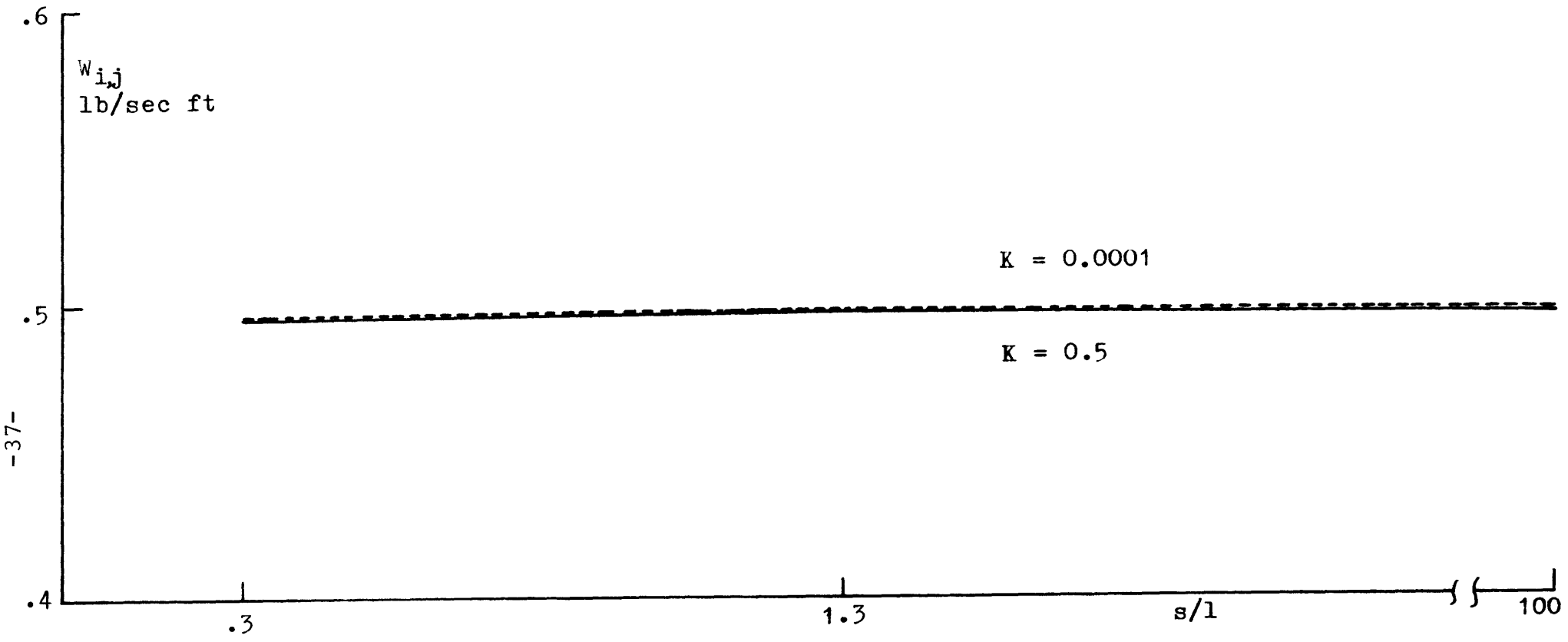

Figure 2.14 Sensitivity of Local Cross Flow to s/l and K for Porous Blockage Condition (Larger Axial Step Length)

Chapter 3
THE COMPARISON OF AVAILABLE DATA WITH ANALYTICAL PREDICTIONS

3.1 Introduction

The thermal analysis of open lattice reactor cores requires a detailed knowledge of coolant flow and properties in each fuel assembly. Prediction of these quantities is difficult since each assembly is free to exchange mass and momentum with its neighbors. Therefore, sufficient experimental data are necessary to assess the analytical predictions. The ideal way to produce data confidently is to perform a scaled simulation of a full sized core. Due to the high cost of such a experiment, and the present lack of facilities, no such experiments have been done. In fact only few measurements have been made in bundle and subchannel test sections.

A survey of published experiments and their comparisons with analytical predictions was made to assess the COBRA predictions. The assessment was done using COBRA because it was selected as the tool of the simplified method.

3.2 Bundle and Subchannel Experiments

In order to achieve improvement in the prediction by the thermal-hydraulic computer code, it is necessary to gain a better understanding of the coolant flow and enthalpy distribution in the complex geometries. Five very completed bundle subchannel experimental works are examined. Comparisons of data with analytical predictions are presented. For detailed information, see References 4 through 8.

3.2.1 Available Data

3.2.1.1 General Electric Data (Data Set 1)

Extensive subchannel test data have been taken in an electrically heated 9-rod bundle under condition typical of BWR operating conditions. Uniform and peaked local (radial) power distributions were both selected. [4]

3.2.1.2 Columbia University Data (Data Set 2)

Simultaneous measurements of flow and enthalpy were made at the exits of two subchannels in a 16-rod electrically heated full-scale model of a typical LWR fuel rod geometry. Experimental data were obtained for conditions of both

subcooled and bulk boiling.[5]

3.2.1.3 Heston Laboratory Data (Data Set 3)

Experiments were made to measure the mixing between subchannels in a uniformly heated 7-rod bundle cooled by boiling Freon-12 at a pressure of 155 psia. Modeling water at 1000psia.[6]

3.2.1.4 CEN-Grenoble Data (Data Set 4)

The experiments are performed in the FRENESIE loop with Freon-12. The 4-rod square array bundle was electrically heated.[7]

3.2.1.5 Pacific Northwest Laboratory Data (Data Set 5)

Laboratory experiments were performed to determine the amount of natural turbulent mixing that occurs between two interconnected parallel channels typical of those in rod bundle. An electrically heated test section which simulates channels formed by rods on a square pitch array located next to rods on a triangular pitch array, was used for the experiments.[8]

3.2.2 Summary of the Five experiments

In order to have a clear view to judge the different

results, the different test sections and conditions are presented. The results shown here are the typical ones for each experiment. All information in this section is extracted from References 4 through 8 and are presented either in tables or by figures.

Tests	Test Sections	Test Conditions	Test Results
General Electric	Fig. 3.1,	Table 3.1	Table 3.6, Table 3.7
Columbia University	Fig. 3.2,	Table 3.2	Fig. 3.6, Fig. 3.7
Heston Lab.	Fig. 3.3,	Table 3.3	Fig. 3.8, Fig. 3.9
CEN-Grenoble	Fig. 3.4,	Table 3.4	Fig. 3.10, Fig. 3.11
Pacific Northwest Lab	Fig. 3.5,	Table 3.5	Fig. 3.12, Fig. 3.13

3.2.3 Comparisons of Results with Analytical Predictions

The following subsections show only significant typical results. For more detailed results, see references mentioned before.

3.2.3.1 Data Set 1

Table 3.6 shows the single phase data and COBRA predictions with β equal to 0.005 and 0.01. For this single phase condition, predictions do agree with data. Table

3.7 shows the comparison under two-phase conditions between data and the predictions with COBRA for β equal to 0.01 and 0.04. Somewhat better agreement is obtained with data for β = 0.04. However, the trends in subchannel qualities are not predicted by the COBRA model.

Even with the high mixing, COBRA cannot predict the substantially lower-than-average qualities in the corner subchannel, and higher-than-average qualities in the center subchannel. In fact, if mixing were made infinitely large the three subchannels would all be at average conditions and thus the data cannot be explained in terms of mixing. Therefore, from G.E. data, COBRA fails to predict accurately when the average exit equilibrium quality is greater than or equal to 0.029.

3.2.3.2 Data Set 2

Figures 3.6 and 3.7 compare the predictions of COBRA II to the experimentally observed flow distributions in subchannel 5 and 11 (Refere to Figure 3.2). These figures indicate that the accuracy of the predicted flow deviation with the homogeneous model is substantially less for conditions of subcooled boiling. The agreement is considerably improved, however, when the Martinelli-Nelson model is employed. This is expected since the Martinelli-Nelson two-

phase pressure drop multiplier is larger than the homogeneous multiplier at the same quality. Therefore, mixing should not be the only effect which needs to be considered to match the data. From this set of data which was performed mainly with subcooled exit conditions, COBRA fails to predict well when the average exit equilibrium quality is greater than zero.

3.2.3.3 Data Set 3

Figure's 3.8 and 3.9 compares the experimental values of ΔP_{12} (exit pressure differences due to inlet flow forced split) with the predicted values at various of F_m using HAMBO Computer Code. (9)

Where F_m: An empirical multiplier of mixing coefficient in HAMBO Code.

It can be seen that under one phase condition predictions match data quite well, but predictions can not match data under two phase conditions. The average exit qualities for all cases shown in Figure 3.9 are greater than 0.012. Therefore, the F_m mixing parameter adjustment does not work if the exit average quality is greater than 0.012.

3.2.3.4 Data Set 4

On Figure 3.10 is presented the variations of mass

velocity relative differences versus the mean outlet thermodynamic quality. Thermodynamic quality distributions between subchannels versus the mean thermodynamic quality are plotted on Figure 3.11. "A" and "K_T" indicated on Figure 3.10 are the adjusting parameters for mixing used in FLICA Computer code. One parameter is for the diffusion of momentum, another one is for the diffusion of enthalpy. Predictions are in good agreement with data when quality is less than zero. But when quality is greater than zero, predictions of subchannel quality can not match data well, even though the prediction of subchannel flow rate matches data. This means that the FLICA code also has trouble to predict accurately for conditions of positive exit equilibrium quality.

3.2.3.5 Data Set 5

Figure's 3.12 and 3.13 are plots of the subchannel enthalpy rise, through the test section and subchannel flow rate versus heat flux for two different channel dimensions. Each figure represents the exit conditions for a simulated rod spacing, flow rate, and inlet temperature. COBRA calculations are also shown on the plots for comparison. Good agreement between data and predictions can be seen from these plots for this two-channel experiment even

under two phase conditions.

3.3 Full Scale Core Experiment

The only attempt to analyze the coolant flow distribution in PWR core from a full scale core experimental data is the work which was done by Henry Herbin.[10] Assembly exit temperature distributions are the only data obtained from an actual plant measurements. Parameters in COBRA IIIC were adjusted to match data. The ranges of parameters used by Herbin are shown in Table 3.8. A typical comparison of COBRA results with data is shown in Figure 3.14. It can be seen that the assembly exit conditions of the coolant are not greatly affected by the values chosen for each parameter. This low sensitivity indicates that the information obtained from the assembly exit thermocouple can not be used for the determination of the cross flow pattern between the fuel assemblies.

3.4 WOSUB Code

This thermal hydraulic computer code is based on a physical model which includes two-phase separated flow model, subcooled boiling, a vapor mixing diffusion model which accounts for the affinity of the vapor to redistribute towards the interior of the bundle, and a recirculation

loop flow concept model. Louis J. Guillebaud,[11] based on the General Electric experimental results concluded that this code can predict better than other subchannel analysis codes under high quality ($0.02 \sim 0.2$) two-phase condition.

A typical comparison plot between WOSUB, COBRA, and G. E. data is shown in Figure 3.15. The predicted subchannal flow suggests that the WOSUB model has promise to better match the G. E. data. For detailed information on the WOSUB code see Reference 11. The method is under development at MIT under Prof. L. Wolf.

TEST CONDITIONS
(p = 1000 psi)

Test Point	Bundle Average Mass Flux $\bar{G} \times 10^{-6}$ (lb/ft^2-h)	Power (kW)	Heat Flux (Btu/ft^2-h)	Subcooling (Btu/lb)	Bundle Average Exit Quality $\bar{x}_e$
1B	0.480	0	0	504.6	–
1C	0.990	0	0	504.6	–
1D	1.510	0	0	504.6	–
1E	1.97	0	0	504.6	–
2B2	0.530	532	225,000	149.9	0.029
2B3	0.535	532	225,000	108.7	0.090
2B4	0.535	532	225,000	52.8	0.176
2C1	1.060	532	225,000	57.2	0.042
2C2	1.068	532	225,000	35.1	0.075
2D1	0.540	1064	450,000	259.2	0.110
2D3	0.540	1064	450,000	124.4	0.318
2E1	1.080	1064	450,000	142.9	0.035
2E2	1.080	1064	450,000	96.7	0.106
2E3	1.060	1064	450,000	29.1	0.215
2F1	2.07	1064	450,000	59.6	0.040
2F2	2.07	1064	450,000	17.4	0.109
2G1	1.07	1596	675,000	225.9	0.038
2G2	1.080	1596	675,000	189.8	0.090
2G3	1.070	1596	675,000	146.7	0.160
2H1	2.12	1560	660,000	102.6	0.031
2H2	2.12	1596	675,000	59.2	0.099
2I2	1.06	1880	800,000	227.5	0.104

Table 3.1 Test Conditions for G.E. Experiment Table 2 of Ref. 4

P	HIN	PW	GAV
500	241	1.44	2.01
500	286	1.48	1.95
500	301	1.48	1.98
500	342	1.53	2.02
500	325	1.53	2.00
500	305	1.52	1.98
500	290	1.53	2.00
500	270	1.52	1.97
1200	172	0.99	1.01
1200	225	0.98	1.02
1200	277	1.00	1.01
1200	304	0.99	1.01
1200	329	0.99	1.02
1200	355	0.99	1.03
1200	395	0.97	1.02
1200	420	0.99	1.00
1200	448	1.00	0.99
1200	367	1.47	0.99
1200	350	1.48	0.94
1200	334	1.50	0.99
1200	302	1.51	0.98
1200	245	1.45	1.01
1200	268	1.46	1.01
1200	292	1.45	1.02
1200	313	1.47	0.98
1200	333	1.48	1.00
1200	354	1.48	1.00
1200	378	1.47	0.99
1200	386	1.49	1.00
1200	271	1.48	0.97
1200	278	1.47	0.99
1200	291	1.46	0.97
1200	303	1.48	1.01
1200	316	1.49	1.01
1200	324	1.49	1.02
1200	397	1.52	0.98
1200	406	1.52	1.01
1200	418	1.52	1.00
1200	430	1.52	0.99
1200	441	1.52	1.01
1200	271	1.50	2.02
1200	302	1.49	1.98
1200	333	1.50	2.00
1200	367	1.50	2.01
1200	399	1.50	2.02
1200	412	1.50	2.02
1200	424	1.49	2.00
1200	435	1.49	2.02
1200	447	1.49	2.03
1200	455	1.48	2.01
1200	466	1.48	1.99
1200	430	1.48	2.01
1200	468	1.47	1.96
1200	484	1.48	2.01
1200	455	1.49	1.97
1200	442	1.50	1.98
1200	430	1.52	2.00

Table 3.2

Continue Next Page

P	HIN	PW	GAV
1200	433	1.48	2.96
1200	320	1.48	3.00
1200	225	1.50	2.99
1200	267	1.45	2.98
1200	321	1.47	3.00
1200	391	1.43	2.95
1200	408	1.53	2.96
1200	429	1.46	2.98
1200	453	1.40	2.95
1200	475	1.49	2.95
1200	336	2.47	2.98
1200	352	2.44	2.97
1200	362	2.45	2.98
1200	369	2.44	2.96
1200	381	2.43	2.97

GAV : Average Mass Velocity ($x10^{-6}$ lb/hr-ft^2)

HIN : Inlet Enthalpy (Btu/lb)

P : System Pressure (psia)

PW : Total Test Section Power (megawatts)

Table 3.2 Test Conditions for Columbia University Experiment

G_o	Q_o	H_1
Mlb/ft^2 hr	Btu/	Btu/lb
0.50	3.75	8.06
1.01	6.74	8.51
1.01	18.84	4.34
1.01	26.99	4.33
1.01	33.67	4.31
1.52	12.84	10.93
1.53	23.82	4.17
1.55	27.07	4.43
1.54	31.78	4.35
1.53	37.68	4.26
2.03	14.43	11.22
2.01	29.22	4.42
2.01	38.67	4.40
2.54	19.36	11.26

Where:

G_o = whole channel mass velocity

Q_o = whole channel power

H_1 = inlet subcooling

Table 3.3 Test Conditions for Heston Lab. Experiment

Outlet absolute pressure: $P = 23.3\ Kg/cm^2$

Mean mass velocity and inlet temperature:

$G = 50\ g/cm^2.s$ $\quad T_i = 60^\circ C$

$G = 85\ g/cm^2.s$ $\quad T_i = 60, 65, 70^\circ C.$

Table 3.4 Test Conditions for CEN-Grenoble Experiment

Pressure	900 psia
Inlet Temperature	330°F (one phase) 510°F (two phase)
Mass Flow Rates	1×10^6 lb/hr-ft^2 2×10^6 lb/hr-ft^2 3×10^6 lb/hr-ft^2
Rod Spacings	0.020 in 0.084 in
Heat Flux	2/3 CHF

Table 3.5 Test Conditions used in Pacific Northwest Lab. Experiment

SINGLE-PHASE (COLD): MEASURED AND PREDICTED MASS FLUXES

Test Point		$\bar{G} \times 10^{-6}$ (lb/ft^2-h)	$G_1 \times 10^{-6}$ (lb/ft^2-h)	$G_2 \times 10^{-6}$ (lb/ft^2-h)	$G_3 \times 10^{-6}$ (lb/ft^2-h)
1B	Data	0.480	0.311	0.462	0.526
	COBRA $\beta = 0.01$	0.480	0.352	0.451	0.551
	COBRA $\beta = 0.005$	0.480	0.336	0.447	0.560
1C	Data	0.990	0.701	0.939	1.150
	COBRA $\beta = 0.01$	0.990	0.740	0.934	1.128
	COBRA $\beta = 0.005$	0.990	0.704	0.925	1.149
1D	Data	1.510	1.095	1.441	1.690
	COBRA $\beta = 0.01$	1.510	1.143	1.427	1.713
	COBRA $\beta = 0.005$	1.510	1.085	1.414	1.746
1E	Data	1.97	1.62	1.91	2.19
	COBRA $\beta = 0.01$	1.97	1.502	1.865	2.229
	COBRA $\beta = 0.005$	1.97	1.424	1.847	2.273

Table 3.6 Comparisons between G.E. Data and COBRA Predictions
Table 8 of Ref. 4

TWO-PHASE: MEASURED AND PREDICTED FLOW AND ENTHALPY DISTRIBUTION

Test Point	$\bar{G} \times 10^{-6}$ (lb/ft^2-h)	$\bar{x}_e$		$G_1 \times 10^{-6}$ (lb/ft^2-h)	$\bar{x}_1$	$G_2 \times 10^{-6}$ (lb/ft^2-h)	x_2	$G_3 \times 10^{-6}$ (lb/ft^2-h)	x_3
2B2	0.530	0.029	Data	0.372	0.003	0.521	0.014	0.540	0.030
			COBRA $\beta = 0.04$	0.482	0.030	0.523	0.026	0.552	0.031
			COBRA $\beta = 0.01$	0.491	0.046	0.516	0.025	0.558	0.029
2B3	0.535	0.090	Data	0.550	0.072	0.530	0.076	0.521	0.104
			COBRA $\beta = 0.04$	0.478	0.090	0.528	0.086	0.560	0.092
			COBRA $\beta = 0.01$	0.454	0.104	0.524	0.084	0.571	0.092
2B4	0.535	0.176	Data	0.524	0.133	0.517	0.180	0.560	0.220
			COBRA $\beta = 0.04$	0.469	0.177	0.526	0.172	0.565	0.178
			COBRA $\beta = 0.01$	0.417	0.194	0.524	0.169	0.581	0.179
2E1	1.080	0.036	Data	0.950	0.004	1.102	0.026	1.162	0.051
			COBRA $\beta = 0.04$	0.990	0.035	1.082	0.031	1.102	0.038
			COBRA $\beta = 0.01$	0.874	0.057	1.068	0.030	1.151	0.034
2E2	1.080	0.106	Data	1.046	0.049	1.078	0.097	1.180	0.105
			COBRA $\beta = 0.04$	0.979	0.106	1.073	0.102	1.117	0.109
			COBRA $\beta = 0.01$	0.878	0.125	1.073	0.099	1.143	0.109
2E3	1.060	0.215	Data	0.965	0.160	1.081	0.185	1.126	0.249
			COBRA $\beta = 0.04$	0.938	0.215	1.044	0.211	1.113	0.217
			COBRA $\beta = 0.01$	0.826	0.234	1.046	0.206	1.140	0.220

Table 3.7 Comparisons between G.E. Data and COBRA Predictions Table 9 of Ref. [4]

Parameters	Range
Axial Node Length	4.2 ∽ 7.9 in.
Flow Convergence Factor	0.005 ∽ 0.020
s/l Parameter	0.10 ∽ 0.5
Turbulent Momentum Factor	0.0 ∽ 0.9
Cross Flow Resistance K	0.1 ∽ 0.9

Table 3.8 Ranges of Adjusting Parameters in COBRA Used by Herbin

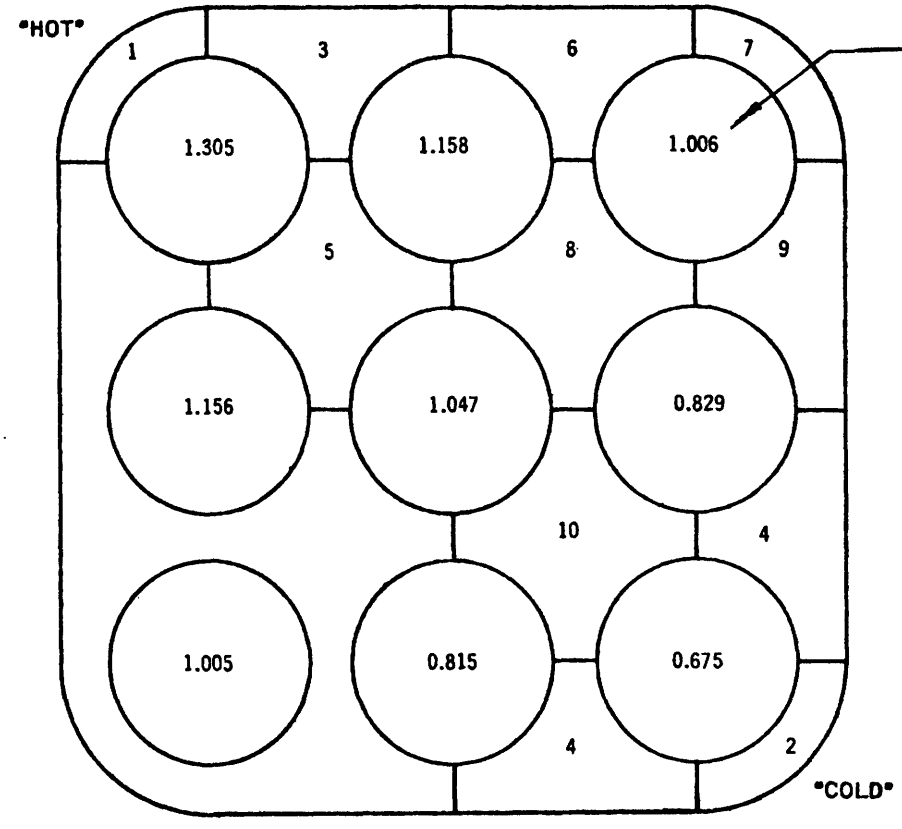

Subchannels and Peaking Pattern

Rod Diameter	0.570 inch
Radius of Channel Corner	0.400 inch
Rod-Rod Clearance	0.168 inch
Rod-Wall Clearance	0.135 inch
Hydraulic Diameter	0.474 inch
Heated Length	72 inches

Figure 3.1 Test Section used in G. E. Experiment
Fig. 60 of Ref. 4

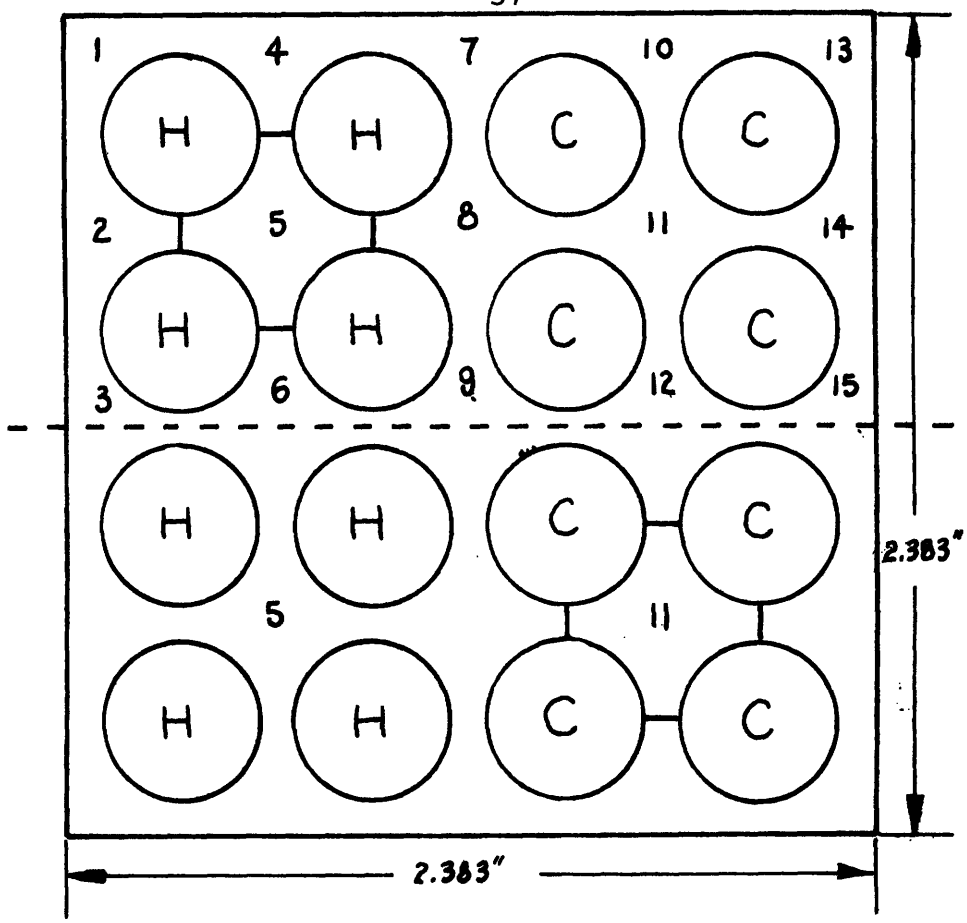

Rod Outside Diameter	0.422 in
Rod Pitch	0.555 in
Rod to Wall Spacing	0.148 in
Rod to Rod Spacing	0.133 in
Total Flow Area	0.02389 Ft^2
Subchannel Area (5, 11)	0.001168 Ft^2
Ratio of Heat Flux	
Hot Rods (H)	100%
Cold Rods (C)	86%
Heated Length	60.0 in

Figure 3.2 Test Section Used in Columbia University Experiment
Fig. 1. of Ref. 5

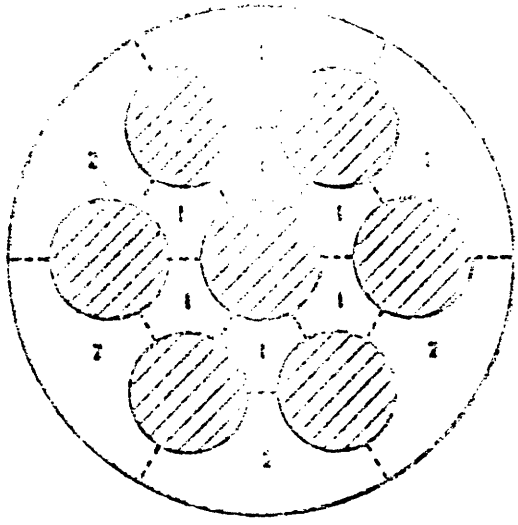

ROD DIAMETER : 0·625 IN.
ROD P.C.D. : 1·375 IN.
SHROUD I.D. : 2·155 IN.
GAP (INNER) : 0·060 IN.
(OUTER) : 0·079 IN.

ENTRY LENGTH (UNHEATED) : 5 IN.
HEATED LENGTH : 36 IN.
CHIMNEY (UNHEATED) : 24 IN.

Figure 3.3 Subchannel Division of 7-Rod Cluster Cross Section Used in the Heston Lab. Experiment Fig. 1 of Ref. 5

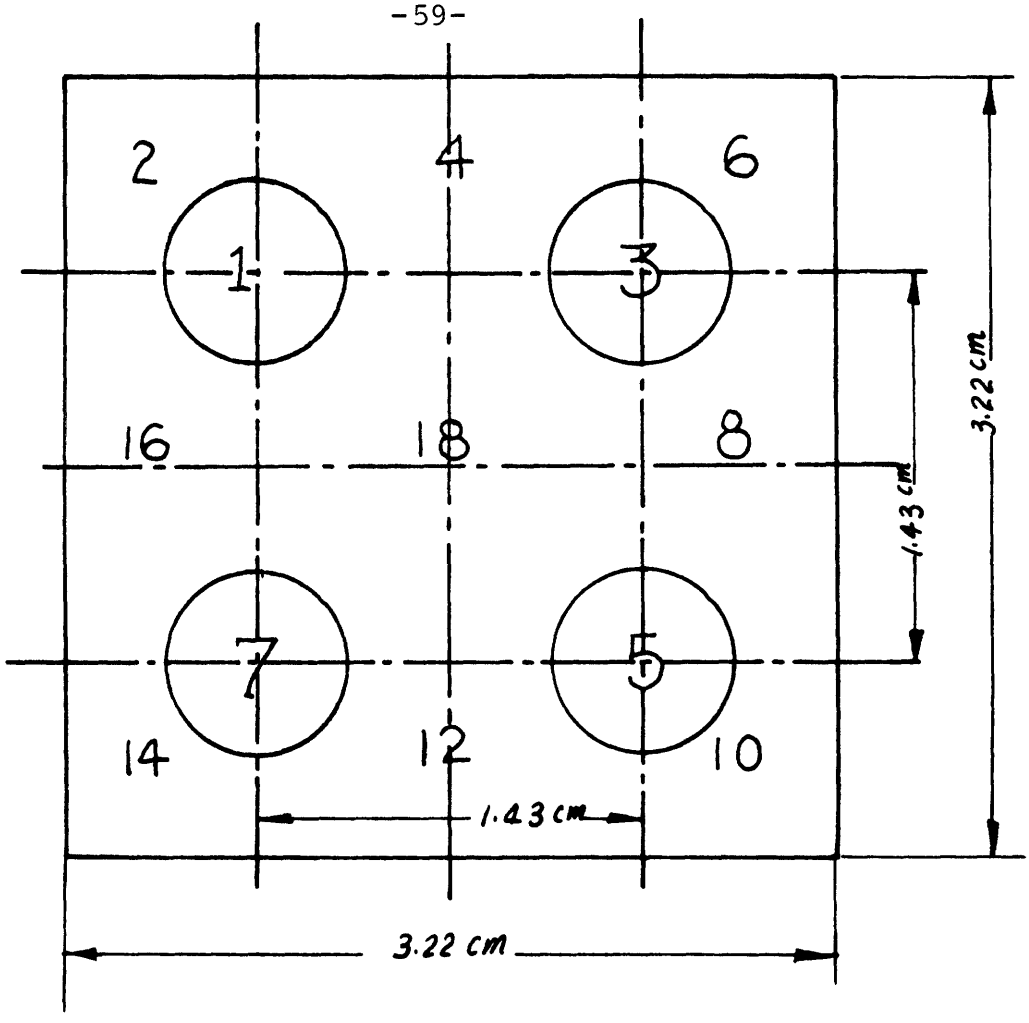

Diameter of the rods: 1.072 cm
Distance between axes of rods: 1.43 cm
(distance between walls of two consecutive rods: 0.358 cm)
Reduced pitch: 1.333 (reduced pitch in the PWR 17 x 17 : 1.325)
Distance between rods and walls: 0.358 cm

	Center Channel	Side Channel	Corner Channel	Total
Cross Sections cm^2	1.142	0.829	0.575	6.758
Hydraulic Dia. cm	1.357	1.064	0.874	1.026

Heating length: 100 cm

Figure 3.4 Test Section Used in CEN- Grenoble Experiment
Fig. 1 of Ref. 7

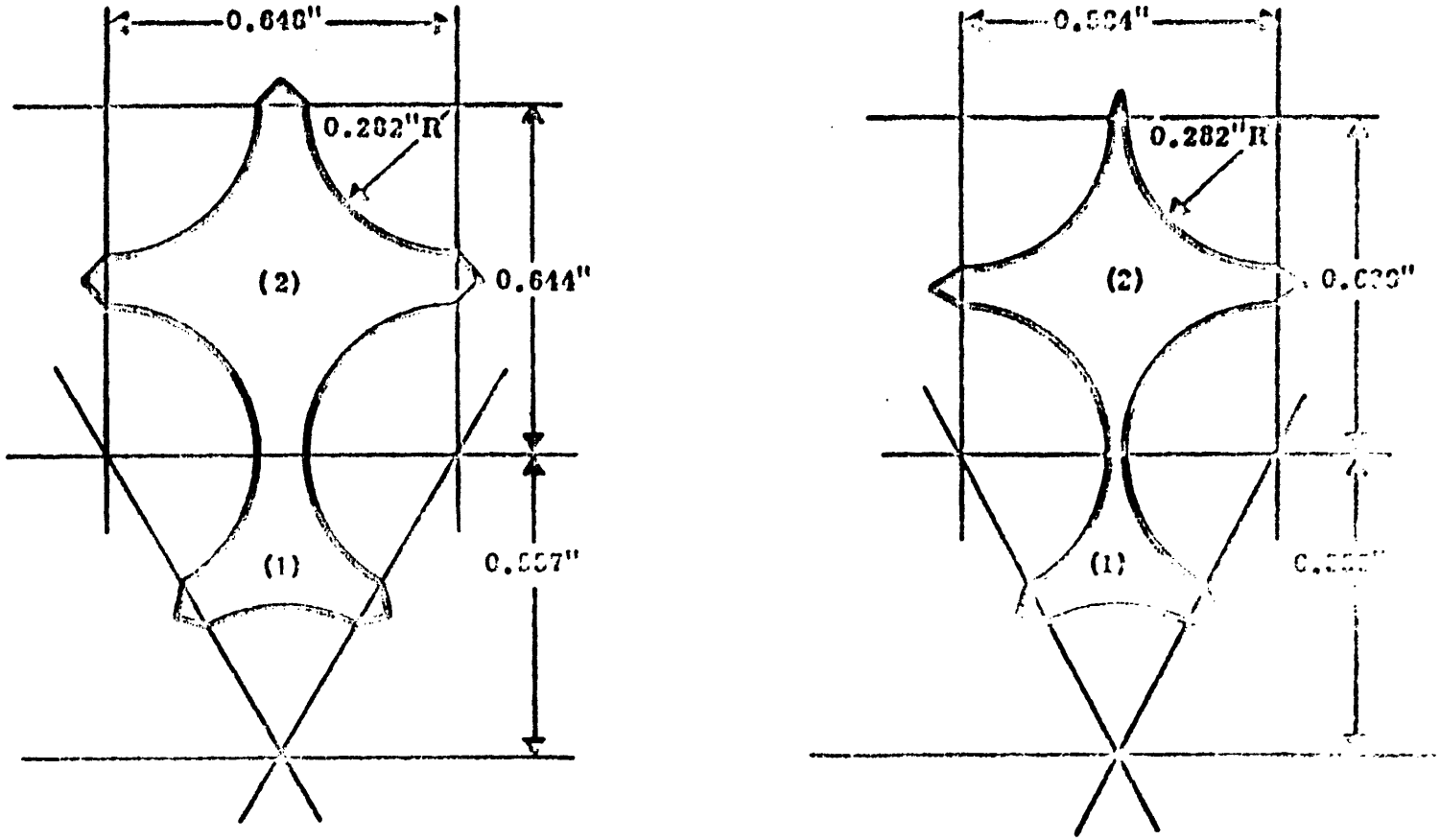

Subchannel Cross Section Dimensions for 0.084 and 0.020 in Simulated Spacing

Figure 3.5 Pacific NorthWest Lab. Experiment Fig 4 of Ref. [8]

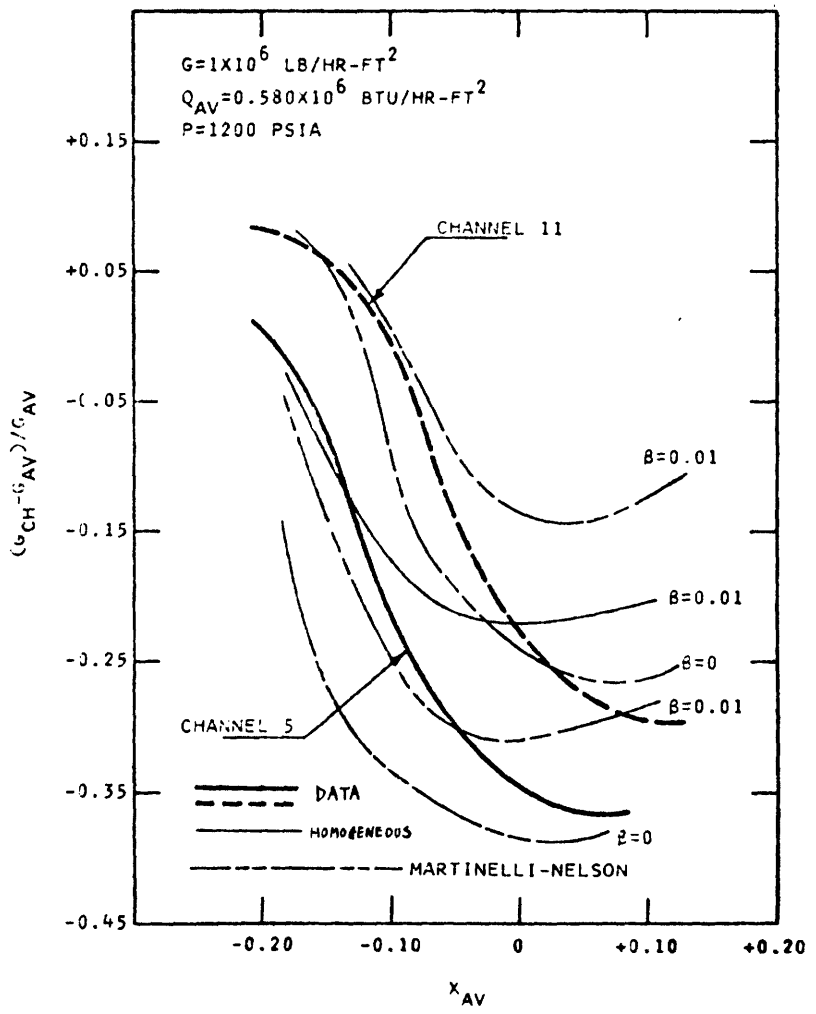

Figure 3.6 Comparison between Columbia University Data and COBRA II Predictions (Normalized Channel Flow Rate Versus Average Quality) Fig. 14 of Ref. 5

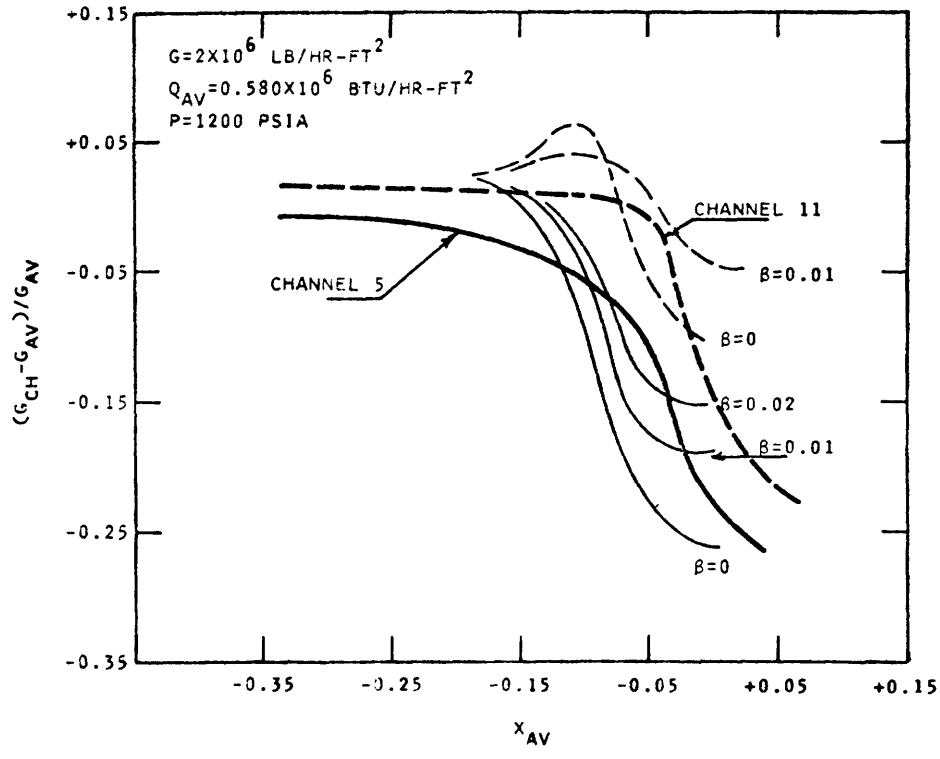

Figure 3.7 Comparison between Columbia University Data and COBRA II Predictions (Normalized Channel Flow Rate Versus Average Quality) Fig. 15 of Ref. 5

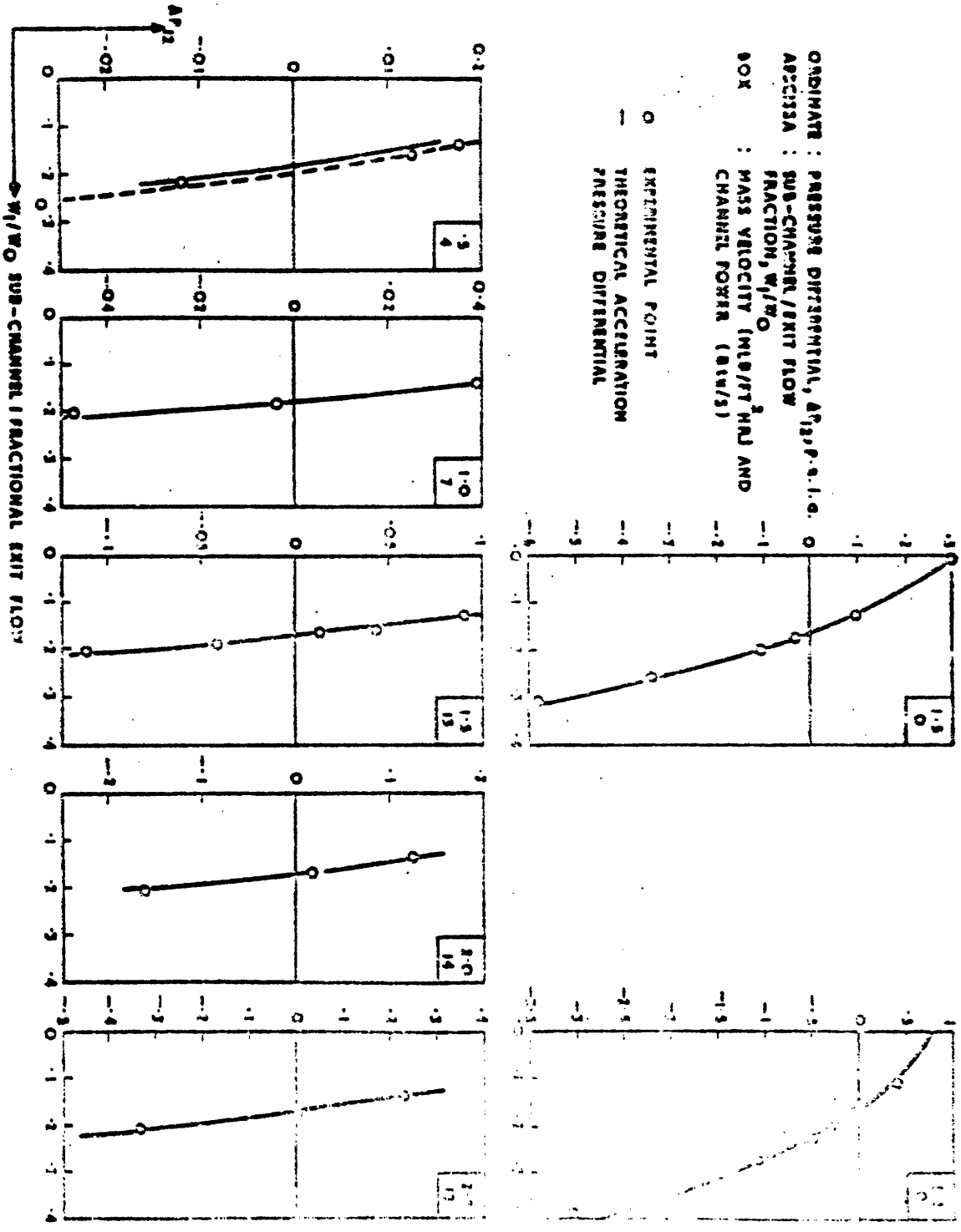

Figure 3.3 SUB-CHANNEL EXIT DIFFERENTIAL PRESSURE (SINGLE PHASE)

Fig. 2 of Ref. 6

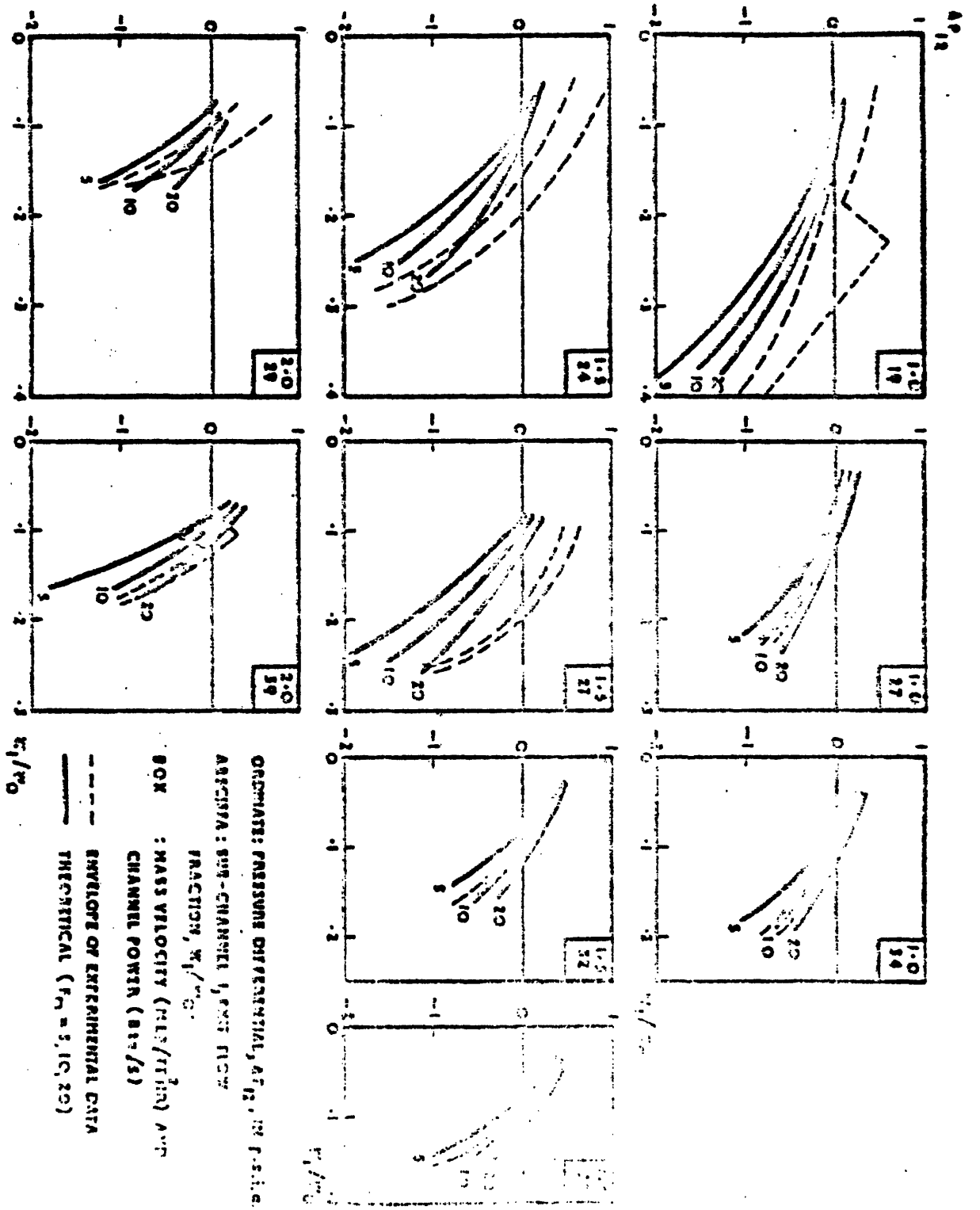

Figure 3.9 SUB-CHANNEL EXIT DIFFERENTIAL PRESSURE (TWO PHASE)

Fig. 3 of Ref. 6

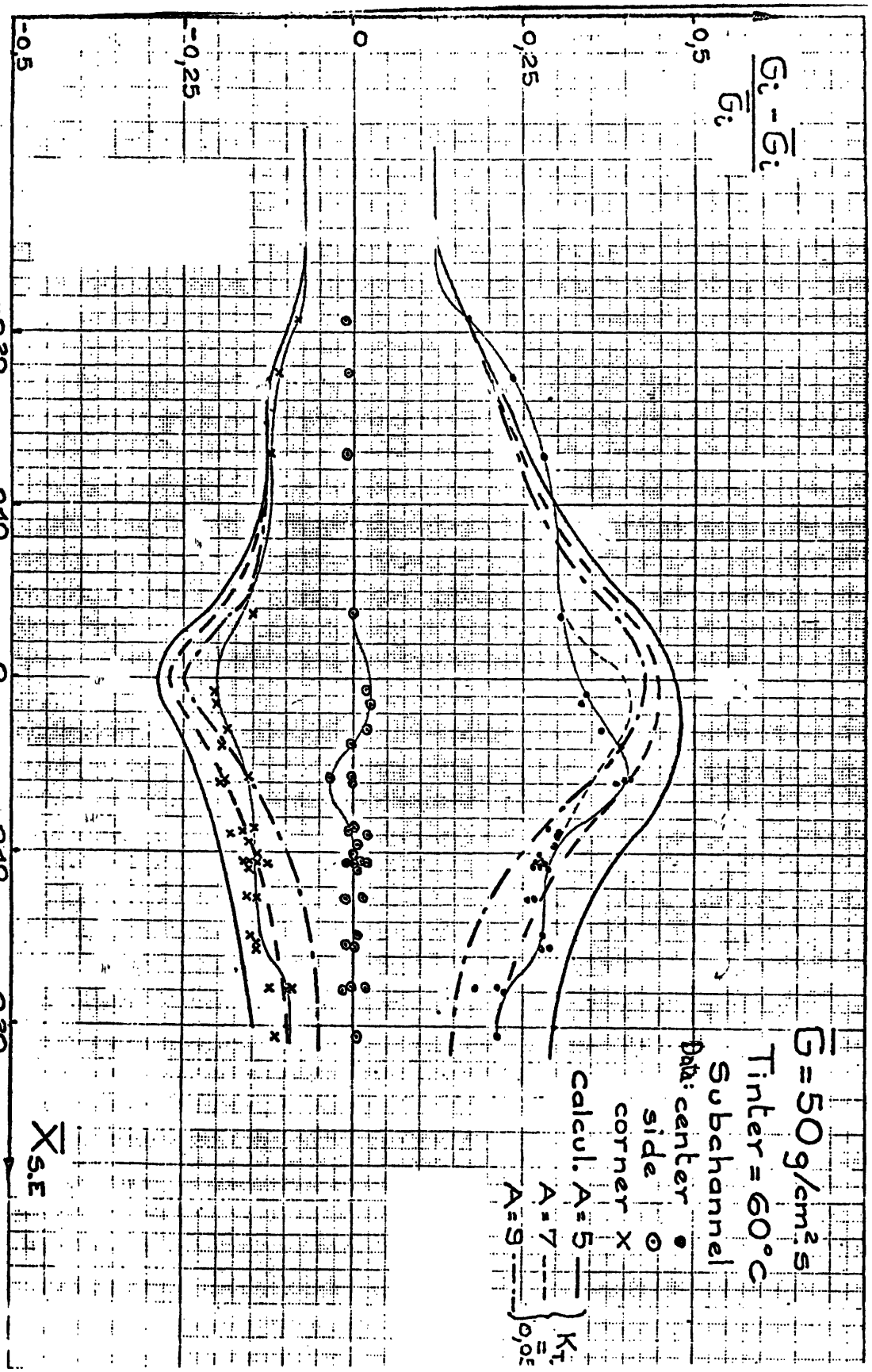

Figure 3.10 Comparison of CEN-Grenoble Experimental Data with FLICA Code (Normalized Channel Flow Rate Versus Average Quality) Fig. 2 of Ref. 7

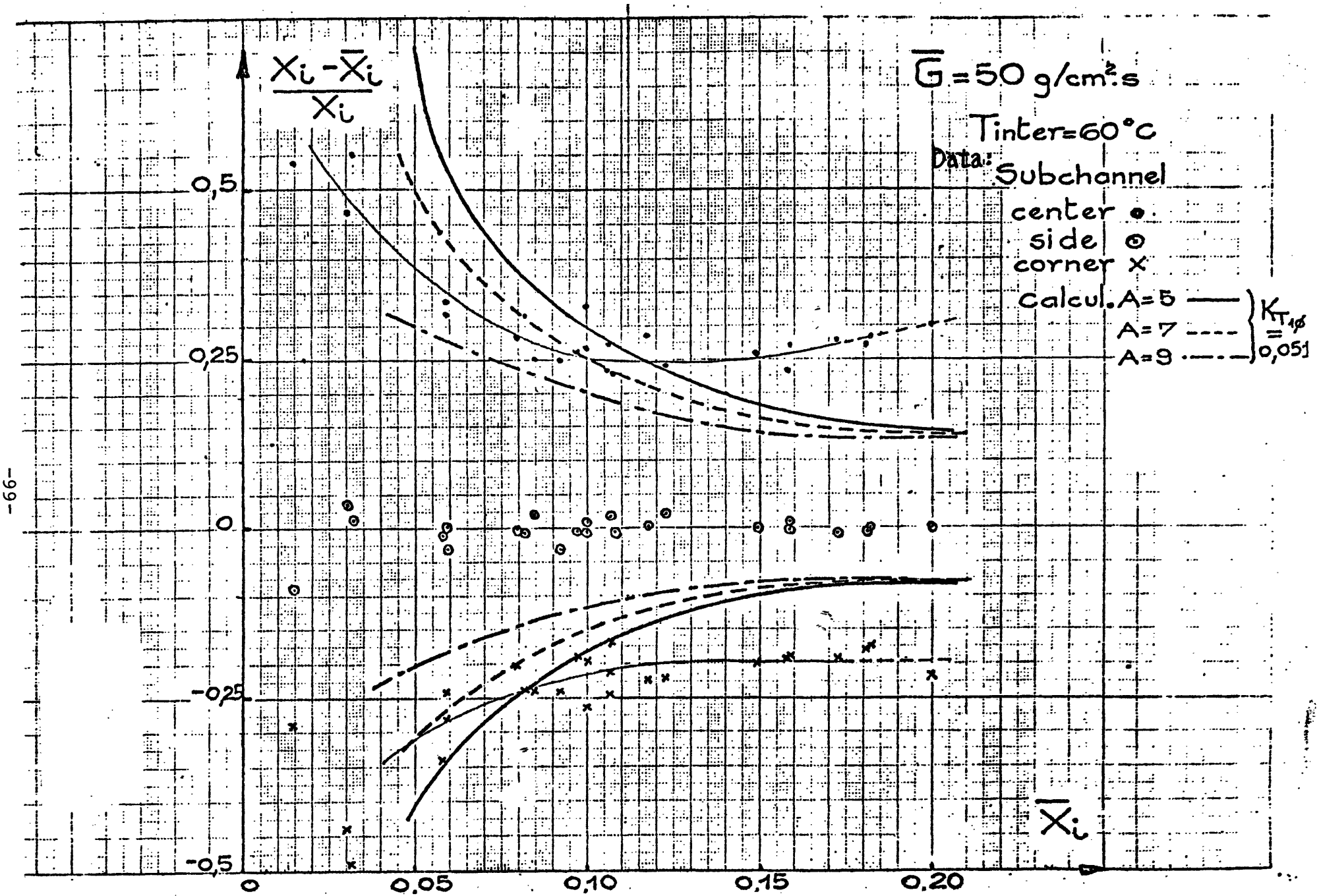

Figure 3 .11 Comparison of CEN-Grenoble Experimental Data with FLICA Code (Normalized Exit Quality versus Average Quality) Fig. 3 of Ref. 7

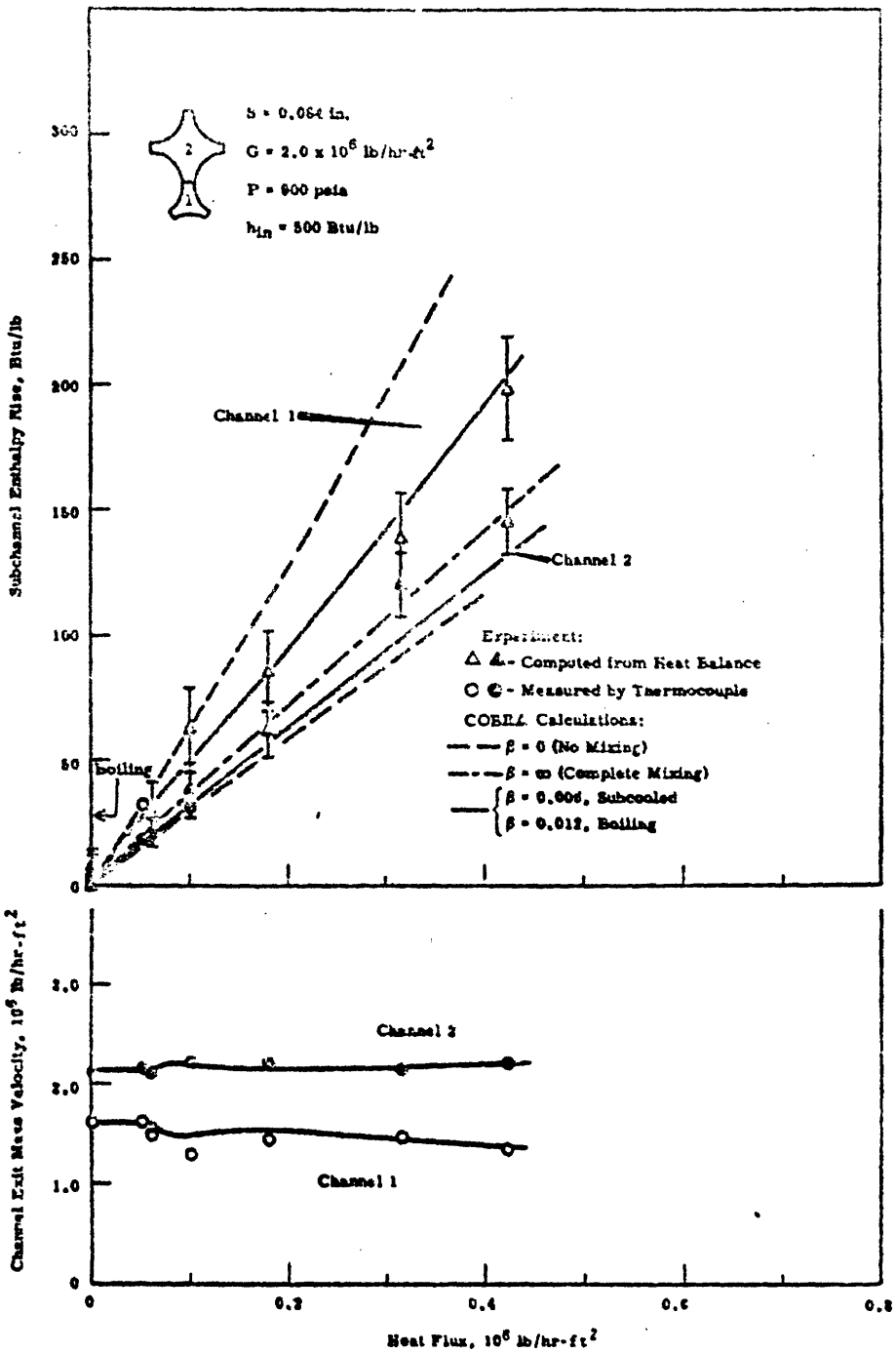

Figure 3.12 *Subchannel Enthalpy Rise and Exit Flow Rate at G = 2.0 x 10^6 lb/hr-ft^2 and 0.084 in. Spacing*
(Comparison of Pacific Northwest Lab. Data with COBRA)

Fig. 12 of Ref. 8

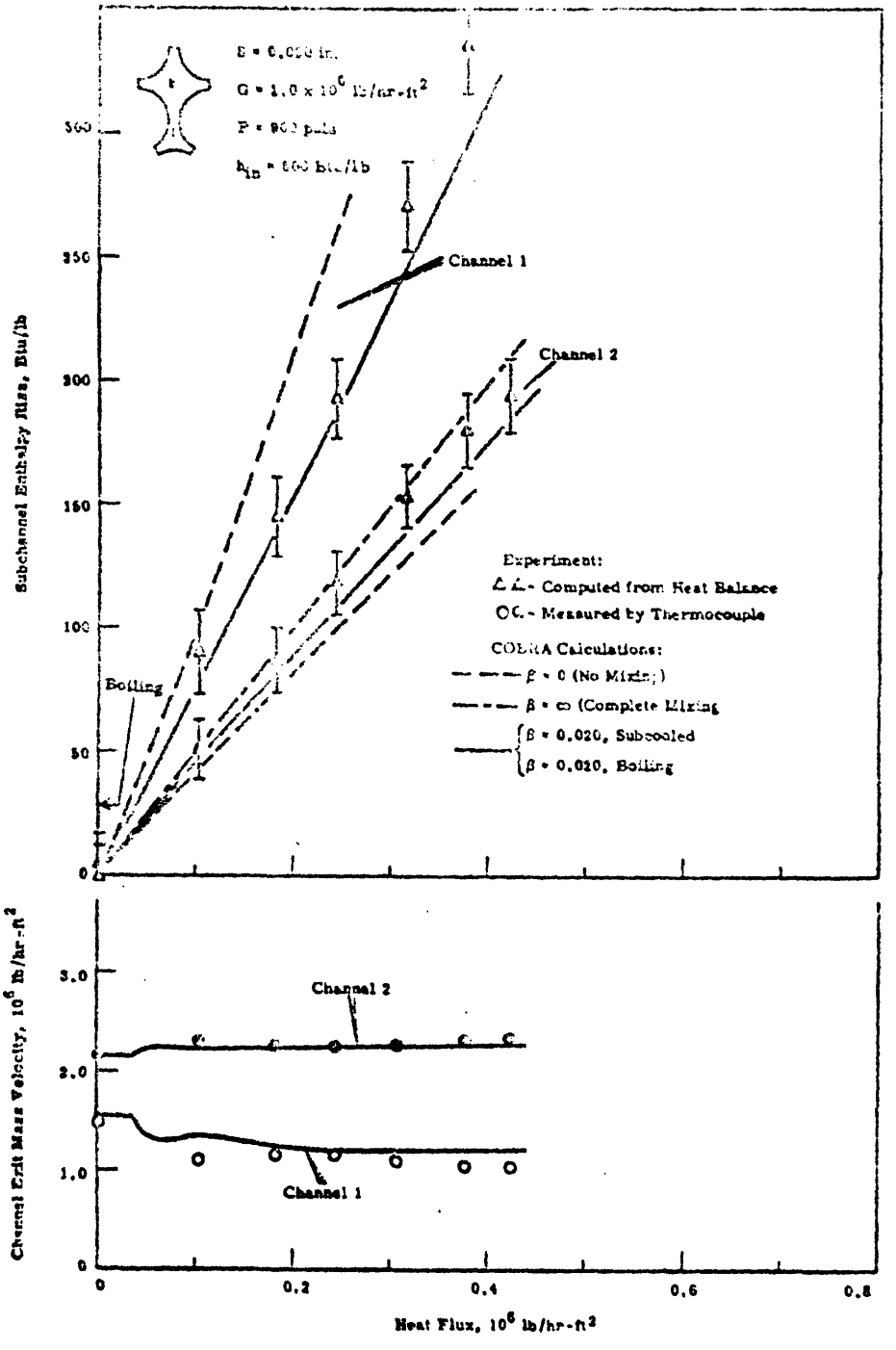

Figure 3.13 *Subchannel Enthalpy Rise and Exit Flow Rate at G = 2.0 x 10^6 lb/hr-ft^2 and 0.020 in. Spacing*
(Comparison of Pacific Northwest Lab. Data with COBRA)

Fig.14 of Ref. 8

	15	14	13	12	11	10	9	8	
R							1.0063	1.0058	1
							1.0063	1.0058	2
							1.0063	1.0058	3
									4
P					1.0051	0.9974	0.9927	1.0044	
					1.0051	0.9974	0.9927	1.0044	
					1.0051	0.9974	0.9927	1.0044	
N				1.0034	0.9906	1.0029	1.0000	0.9997	
				1.0034	0.9906	1.0029	1.0000	0.9997	
				1.0034	0.9906	1.0029	1.0000	0.9997	
M				0.9980	0.9940	0.9952	0.9954	1.0066	
				0.9980	0.9940	0.9952	0.9954	1.0066	
				0.9980	0.9940	0.9952	0.9954	1.0066	
L					1.0028	0.9996	1.0024	0.9986	
					1.0028	0.9996	1.0024	0.9986	
					1.0028	0.9996	1.0024	0.9986	
K						0.9980	0.9980	1.0076	
						0.9980	0.9980	1.0076	
						0.9980	0.9980	1.0076	
J							1.0050	1.0015	
							1.0050	1.0015	
							1.0050	1.0015	
H								1.0098	
								1.0098	
								1.0098	

Hottest assembly= N 11

1: Calculated value for cross flow resistance K = 0.1 (case n° 10)

2: Calculated value for cross flow resistance K = 0.5 (reference case)

3: Calculated value for cross flow resistance K = 0.9 (case n° 11)

4: -

0.9934	0.9781
0.9934	0.9781
0.9934	0.9781
0.9781	0.9786
0.9781	0.9786
0.9781	0.9786

Hot subchannels

Figure 3.14 Comparison of the normalized outlet flow distribution as a function of the cross flow resistance.
Fig. 20 of Ref. 10

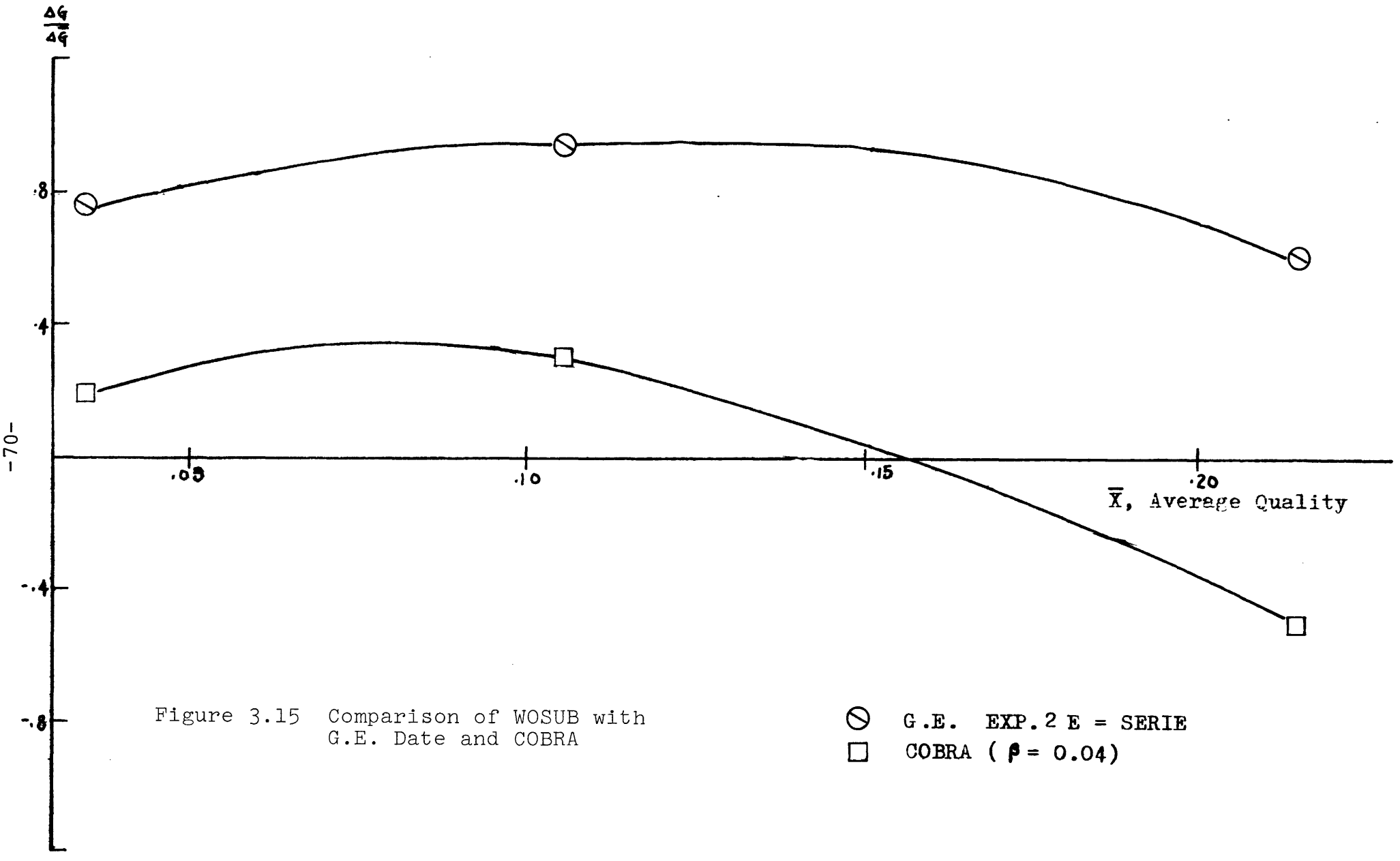

Figure 3.15 Comparison of WOSUB with G.E. Date and COBRA

Chapter 4

CONCLUSIONS

4.1 Effects of s/l and K

Generally speaking, parameters of s/l and K have very little effect on the thermal analysis results obtained from the COBRA IIIC code. Only when the transverse momentum equation plays an important role (e.g. channel has a porous blockage, inlet flow upset), do s/l and K have a large effect on the value of the local cross flow.

The overall thermal analysis results (e.g. enthalpy, MDNBR) would depend primarily on the total cross flow between cases with different values of s/l and K are very small, the overall thermal analysis results are very close no matter what value of s/l or K has been used.

For large axial step length, the effects of s/l and K are even harder to detect.

Therefore, for normal operation condition (no flow upset), large axial step length (for economical reason), the sensitivity to s/l and K is negligible.

This does not mean that these parameters are not important. A precise value of s/l or K is required at least

to reflect the real local situation. Especially due to different local cross flow, the magnitude of MDNBR might be the same but the location of MDNBR may change. Also small axial step length is needed to get better results.

4.2 Accuracy of Analytical Predictions

Single-phase predictions of COBRA agree quite well with data. The bulk quality ($X_e > 0.02$) flow predictions do not agree with the trends in data. For subcooled boiling, COBRA can not predict very accurately when the exit average quality becomes greater than zero. Therefore, the COBRA two phase model has an inherent defect for these conditions. It is evident that without modification of the thermal-hydraulic physics in these codes, agreement with actual data under this condition can not be achieved.

Significant bulk quality coolant flow in PWR core does not occur under normal operating conditions. But it is possible to occur under severe accident transients. Therefore, a code which can predict high quality two phase trend for PWR core is still needed. From this study it is clear that the WOSUB physical model has promise to perform better than COBRA model under significant bulk quality conditions.

Also this study shows that COBRA can predict better for the simulated subchannel conditions than it does for the actual multirod conditions. This implies that the magnitude of the transfer mechanism of the coolant is different between these two geometries. This effect was already demonstrated in Reference 1, Figure 3 where it was shown that results are quite different (10% difference) due to whole core or partial core analysis. Owing to this, data obtained from simulated subchannels or actual multi-rod bundles cannot be used with high confidence (reduce error to less than 10%) to assess the prediction of an actual subchannel which is placed in an actual PWR core. Therefore, one should be careful to examine the data base in this regard for assessment of analytical predictions.

Actually the mixing should depend on local conditions and should thus vary in the axial direction. Figure 4.1 shows recent measurements of the mixing parameter β as a function of quality for a fixed flow rate.[12] A constant value of β therefore cannot be used to adjust the predictions against data. Also for a large open lattice PWR core, especially under two phase condition, consideration of only mixing is not enough. Other effects like diversion cross flow might have major role in determining the analytical predictions. More experiments are needed, especially scaled simulation of full size core (at least) should be performed to gain better understanding of the coolant transfer mechanism.

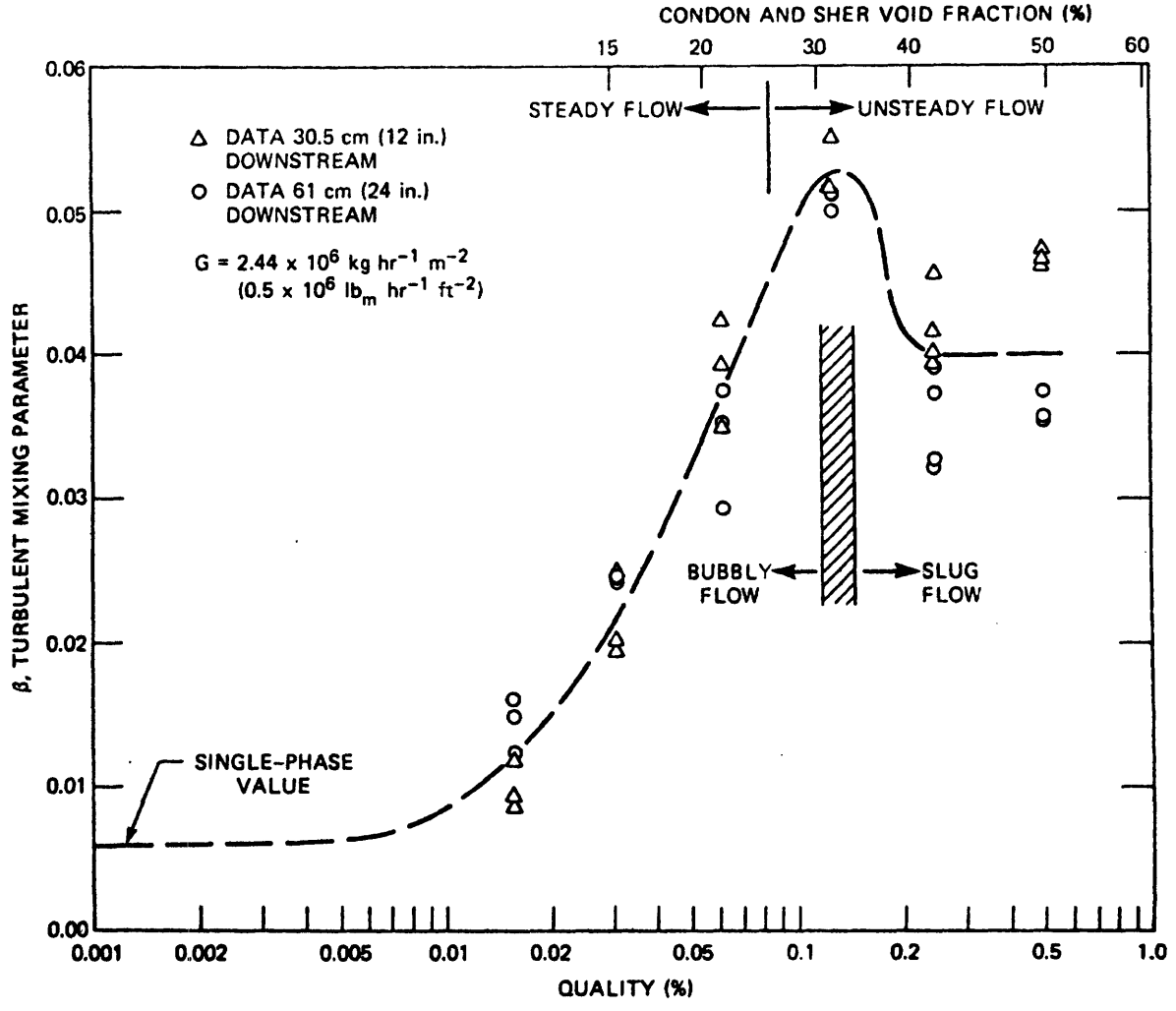

Figure 4.1 Variation of turbulent mixing parameters with quality for a flow rate of 2.44×10^6 kg hr^{-1} m^{-2}. Fig. 4.1 of Ref. 12

REFERENCES

(1) P. Moreno, C. Chiu, R. Bowring, E. Khan, J. Liu, N. Todreas "Methods for Steady State Thermal/Hydraulic Analysis of Pressurized Water Reactor Cores" Energy Laboratory Report No. MIT-EL 76-006, March 1977.

(2) Donald Rowe, COBRA IIIC, BNWEL-1695, Pacific Northwest Laboratories, 1973.

(3) John G. Bartzis, Neil E. Todreas "The Transverse Momentum Balance in Subchannel Analysis" to be submitted to NSE derived from Bartzis S.M. thesis.

(4) R. T. Lahey Jr., B. S. Shiralkar, D. W. Radcliffe "Two-Phase Flow and Heat Transfer in Multirod Geometrics" GEAP-13049, March 1970.

(5) Frank S. Castellana and Joseph E. Casterline "Subchannel Flow and Enthalpy Distributions at the Exit of a Typical Nuclear Fuel Core Geometry" Nuclear Engineering and Design 22 (1972) 3-18, p. 3.

(6) R. W. Bowring, J. Levy "Freon 7-Rod Cluster Subchannel Mixing Experiments" A.P.C. Heston Laboratories AEEW-M906, 1969.

(7) M. Bayoumi, R. Charlot, R. Ricque "Determination of Mass Flow Rate and Quality Distributions Between the Subchannels of a Heated Bundle" European Two Phase Flow Meeting. Erlangen, 31 May - 4 June 1976.

(8) D. S. Rowe, C. W. Angle "Cross Flow Mixing Between Parallel Flow Channels During Boiling Part II Measurement of Flow and Enthalpy in Two Parallel Channels" Pacific Northwest Laboratory, BNN-371 PT2 Dec. 1967.

(9) R. W. Bowring, "HAMBO: A Computer Programme for the Subchannel Analysis of the Hydraulic and Burnout Characteristics of Rod Clusters." Part 2 - The Equations AEEW-R 582 (Jan. 1968).

(10) Henry C. Herbin "Analysis of Operating Data Related to Power and Flow Distribution in a PWR" Nuclear Engineering Thesis M.I.T. June, 1974.

(11) Louis J. Guillebaud "Vapor Diffusion in BWR Fuel Rod Bundles" Nuclear Engineer Thesis M.I.T. January 1977.

(12) P. A. Jallouk "Bundle Hydraulics" ORNL/NURZG/TM-92 p. 22.

(13) I. E. Idel'chik "Handbook of Hydraulic Resistance" A.E.C. 1960. (TR-663).

(14) E. U. Khan, K. Kim, G. D. Lindstrom "Cross Flow Resistance and Diversion Cross Flow Mixing Between Rod Bundles" Trans. Am. Nucl. Soc., 14, 249 (1971).

(15) J. Liu, N. Todreas, "Transient Thermal Analysis of PWR's by a Single Pass Procedure Using a Simplified Nodal Layout" MIT-EL 77-008. June 1977.

Appendix A

SIMULATION OF A POROUS CHANNEL BLOCKAGE

The axial pressure drop due to the existence of the fuel bundle grid spacer is included in the axial momentum equation of the COBRA IIIC computer code. The real PWR spacer loss coefficient may range from 0.5 to 5. generally, it is a function of Reynolds number, and may be written as

$$K_G = a\, R_e^{-b}$$

Where a and b can be determined empirically. The simulation of a porous channel blockage thereforely, can be accomplished by selecting a suitable value of the spacer loss coefficient in such a way that the pressure drop due to the grid spacer is similar to the pressure drop due to the existence of a porous blockage. To fulfill this purpose unrealistic values of K_G may be applied.

For flow through a thick-edged ($1/D_h > 0.015$) orifice in a straight conduit, if $R_e = \frac{W_o D_h}{\nu} > 10^5$, the resistance coefficients ζ is as follows:[13]

$$\zeta = \frac{\Delta H}{\frac{rW^2_1}{2g}} \cong \left[(0.5 + \tau\sqrt{1 - \frac{F_o}{F_1}})\,(1 - \frac{F_o}{F_1}) + (1 - \frac{F_o}{F_1})^2 + \lambda \frac{1}{D_h} \right] (\frac{F_1}{F_o})^2$$

$$= (\zeta_o + \lambda \frac{l}{D_h}) \ (\frac{F_1}{F_o})^2 \qquad \text{(A-1)}$$

$$D_h = \frac{4F_o}{\Pi_o} \qquad \text{(A-2)}$$

$$\tau = f(\frac{l}{D_h}) \quad \text{Which is determined from Table A.1} \qquad \text{(A-3)}$$

Where

F_o: area of the narrowest section of the stretch of the orifice,

F_1: area of the channel section before the narrow section of the stretch of the orifice,

Π_o: section perimeter,

D_o: diameter of the narrowest section of the orifice,

D_h: hydraulic diameter, 4 x hydraulic radius,

l : length of the stretch, depth of the orifice,

W_o: mean stream velocity in the narrowest section of the orifice

W_1: mean stream velocities in the sections before and behind the orifice,

ΔH: pressure loss or resistance of the stretch

Therefore, for any given ratios of F_o/F_1 and $\frac{l}{D_h}$, ζ can be found from the above relations. For example,

suppose that the dimensions of the blockage are such that the ratio of $\frac{l}{D_h}$ equals one (Refer to Figure A.1). The value of ζ which corresponds to a ratio of $F_o/F_1 = 0.40$ snould be 5. (See Table A.1) In addition to this, other values of ζ are listed in Table A.1.

From Table A.1, for a certain spacer loss coefficient K_G, say $K_G = 5$, which is an input to the COBRA IIIC code, a blockage geometry for $\frac{l}{Dh} = 1$ can be obtained as $F_o/F_1 = 0.40$. This means that a 60% of total flow is blocked. The above correspondence of F_o/F_1 which were used in this study to K_G for $\frac{l}{D_h} = 1$ and 4 are listed in Table A.2. For example, if $\frac{l}{D_h} = 1$, $K_G = 25$ corresponds to a condition that 78% of the total flow are blocked. Additionally, value of $\frac{l}{D_h}$ of a real PWR spacer was evalueated. As shown in Figure A.2, for the geometry of a 14 x 14 PWR rod bundle spacer, the value of $\frac{l}{D_h}$ may be assumed to be 4 (Exactely detailed dimensions of the PWR grid are classified information). From Table A.2, for $K_G = 5$, thickness of the spacer (0.3") can be found out. It means that 58.3% of the total flow are blocked for this real PWR spacer condition.

Therefore, Table A.2 gives the values of K_G which corresponds to a simulated channel porous blockage condition.

Values of ζ

$\frac{l}{D_h}$	F_o/F_s																
	∞	0.02	0.04	0.06	0.08	0.10	0.15	0.20	0.25	0.30	0.40	0.50	0.60	0.70	0.80	0.90	1.0
0	1.35	7 000	1 670	730	400	245	96.0	51.5	30.0	18.2	8.25	4.00	2.00	0.97	0.42	0.13	0
0.2	1.22	6 600	1 600	687	374	230	94.0	48.0	28.0	17.4	7.70	3.75	1.87	0.91	0.40	0.13	0.01
0.4	1.10	6 310	1 530	660	356	221	89.0	46.0	26.5	16.6	7.40	3.60	1.80	0.88	0.39	0.13	0.01
0.6	0.84	5 700	1 380	590	322	199	81.0	42.0	24.0	15.0	6.60	3.20	1.60	0.80	0.36	0.12	0.01
0.8	0.42	4 680	1 130	486	264	164	66.0	34.0	19.6	12.2	5.50	2.70	1.34	0.66	0.31	0.11	0.02
1.0	0.24	4 260	1 030	443	240	149	60.0	31.0	17.8	11.1	5.00	2.40	1.20	0.61	0.29	0.11	0.02
1.4	0.10	3 930	950	408	221	137	55.6	28.4	16.4	10.3	4.60	2.25	1.15	0.58	0.28	0.11	0.03
2.0	0.02	3 770	910	391	212	134	53.0	27.4	15.8	9.30	4.40	2.20	1.13	0.58	0.28	0.12	0.04
3.0	0	3 765	913	392	214	132	53.5	27.5	15.9	10.0	4.50	2.24	1.17	0.61	0.31	0.15	0.06
4.0	0	3 775	930	400	215	132	53.8	27.7	16.2	10.0	4.60	2.25	1.20	0.64	0.35	0.16	0.08
5.0	0	3 850	936	400	220	133	55.5	28.5	16.5	10.5	4.75	2.40	1.28	0.69	0.37	0.20	0.10
6.0	0	3 870	940	400	222	133	55.8	28.5	16.6	10.5	4.80	2.42	1.32	0.70	0.40	0.21	0.12
7.0	0	4 000	950	405	230	135	55.9	29.0	17.0	10.9	5.00	2.50	1.38	0.74	0.43	0.23	0.14
8.0	0	4 000	965	410	236	137	56.0	30.0	17.2	11.2	5.10	2.58	1.45	0.78	0.45	0.25	0.16
9.0	0	4 080	985	420	240	140	57.0	30.0	17.4	11.4	5.30	2.62	1.50	0.80	0.50	0.28	0.18
10	0	4 110	1 000	430	245	146	59.7	31.0	18.2	11.5	5.40	2.80	1.57	0.89	0.53	0.32	0.20

Table A.1 From Page 140 of Ref. [13]

$\frac{l}{D_h}$	K_G		
	25	5	2.5
1	0.22	0.40	0.55
4*	0.212	0.417	0.489

* Real PWR Spacer Geometry.

Table A.2 Values of F_o/F_1

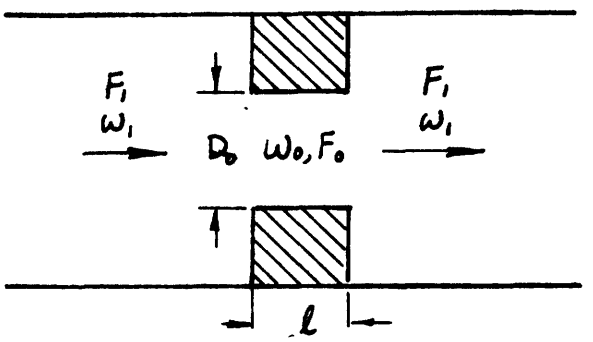

Figure A.1 Simulated Porous Blockage Geometry

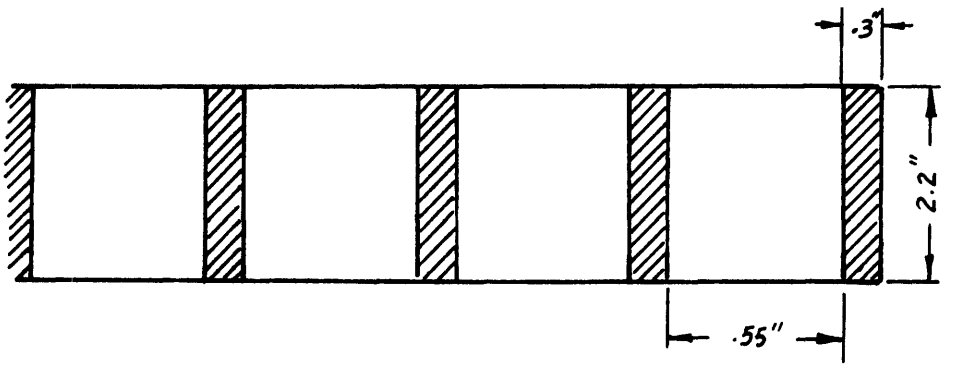

Figure A.2 Estimated PWR Spacer Geometry

APPENDIX B

CROSS FLOW RESISTANCE COEFFICIENT

The purpose of this appendix is to discuss the definition of the cross flow resistance coefficent and the derivation of the recommended value for this coefficient.

Pressure difference (ΔP) between two adjacent subchannels has generally been related to the cross flow velocity v by

$$P = \frac{K \rho v |v|}{2gc} \qquad (B.1)$$

Where K is the cross flow resistance coefficient.

Two conditions have generally been utilized to evaluate K: (a) pure cross flow between rod bundles;

(b) combined flow of axial flow and cross flow.

The transverse momentum equation used in COBRA IIIC may be written in terms of K as: [2]

$$\frac{\partial W_{i,j}}{\partial t} - \frac{\partial (u^* W_{i,j})}{\partial x} = \frac{S}{l}(P_i - P_j) - \frac{K |W| W}{2 S \rho^* l} \qquad (B\text{-}2)$$

Since the axial flow inertia effect is included in the above equation (second term), the cross flow resistance coefficient K used in eq. B-2 does not include the axial inertia effect. The numerical values of K used in eq. B-2 should be evaluated at condition (a) which was mentioned before as the pure cross flow condition.

Values of cross flow resistance coefficient including axial inertia effect for rod bundle were reported by Khan.[14] The results are shown in Figure B.1 as a function of the lateral to axial velocity ratio (v/u'). Since effect of axial inertia is included, all these values of K in Figure B-1 can not be used except at very large value of v/u* for COBRA IIIC. At large values of v/u* Khan's result reduces to $K \approx 0.25$ which would presumable be an estimate of the friction coefficient for pure cross flow.

$K \approx 0.25$ also can be confirmed by another calculation as follows.

For pure cross flow across rod bundles, the cross flow resistance coefficient may be written as:

$$K = A\, R_e^{-0.2} \qquad \text{(B-3)}$$

Where: R_e is the Reynolds number

A is a function of the pitch to diameter ratio.

$$A = \alpha \left(\frac{P}{D}-1\right)^{-0.5} \qquad \text{(B-4)}$$

α = 1.52 which is recommended in Reference 13.

For typical reactor coolant flow, cross flow with Reynolds number which is in the magnitude of 10^5 is usual. For example, a local cross flow with a value of 6.0 lbm/sec-ft across a .1333 inches rod gap will end up with a Reynolds number of 5. x 10^5. Also for a typical PWR bundle, $\frac{P}{D}$ is around 1.3. From the equations above K was evaluated to be 0.27 which is close to the value of 0.25 obtained by Khan's experiment.

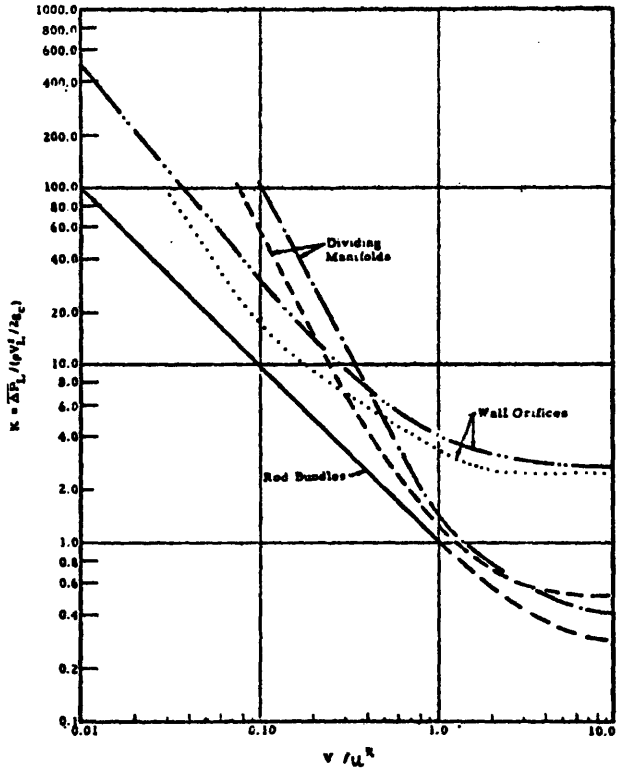

Figure B.1 **Comparison of cross flow resistance coefficient for rod bundles with those of manifold and wall orifices.** (Ref. 14)